

Study of Form Factors and Observables in $B_c^- \rightarrow D_s^{*-} \ell^+ \ell^-$ and $B_c^- \rightarrow D_s^{*-} \nu \bar{\nu}$ decays

Utsab Dey,^a Soumitra Nandi.^a

^a*Department of Physics, Indian Institute of Technology Guwahati,
 North Guwahati, Assam-781039, India,*

E-mail: utsab_dey@iitg.ac.in, soumitra.nandi@iitg.ac.in

ABSTRACT: We investigate the decays $B_c^- \rightarrow D_s^{(*)-} \ell^+ \ell^-$ and $B_c^- \rightarrow D_s^{(*)-} \nu \bar{\nu}$ within the Standard Model (SM), employing perturbative QCD form factors that are sensitive to the wave functions of B_c and $D_s^{(*)}$ mesons. We determine the shape parameters of these mesons and the $B_c \rightarrow D_s^{(*)}$ form factors at $q^2 = 0$ from available lattice QCD inputs for $B_s \rightarrow D_s^{(*)}$ and $B_c \rightarrow D_s$ transitions. To obtain the q^2 dependence of the $B_c \rightarrow D_s^*$ form factors, we employ heavy-quark spin symmetry and an appropriate parametrisation scheme over the allowed q^2 region. Based on these inputs, we present predictions for branching ratios and lepton-flavour-sensitive observables. Furthermore, we perform a detailed angular analysis of the cascade decay $B_c^- \rightarrow D_s^{*-} (\rightarrow D_s^- \pi^0) \ell^+ \ell^-$, providing Standard Model predictions for several angular observables.

KEYWORDS: Bottom Quarks, Semi-Leptonic Decays, Rare Decays

Contents

1	Introduction	1
2	Theoretical Background	3
2.1	Physical Observables	3
2.1.1	Decay widths and branching fractions	3
2.1.2	Angular analysis of rare $B_c^- \rightarrow D_s^{*-} \ell^+ \ell^-$ channel	5
2.2	Form Factors	8
2.3	Light Cone Distribution amplitudes	11
3	Extraction of LCDA shape parameters and form factors at $q^2 = 0$	12
4	Obtaining form factor information over full physical q^2 range	17
4.1	Connecting $B_c \rightarrow D_s^*$ with $B_c \rightarrow D_s$ form factors	17
4.2	Extracting the universal functions Σ_1 and Σ_2	19
4.3	Obtaining q^2 distribution of rest of the $B_c \rightarrow D_s^*$ form factors	22
5	Prediction of physical observables	28
5.1	Decay Width and branching fractions	28
5.2	Angular Observables	29
6	Summary and Conclusions	36
A	Expressions of various transversity amplitudes in $B_c^- \rightarrow D_s^{*-} \ell^+ \ell^-$	37
B	Expressions of form factors in PQCD approach	39
C	Scales and relevant functions in the hard kernel	42
D	Inputs utilized in this work	43
E	Correlation matrices	45

1 Introduction

The study of semileptonic and leptonic decays of B mesons is crucial for determining the Cabibbo-Kobayashi-Maskawa (CKM) matrix elements and probing possible scenarios of New Physics (NP). Among the key observables, lepton flavor universality (LFU) ratios play a central role, as they test a fundamental prediction of the Standard Model (SM) that interactions involving different charged-lepton flavors are identical up to mass effects.

The B_c meson has emerged as an important subject in flavor physics. First observed by the CDF Collaboration at the Tevatron in 1998 through the semileptonic decay $B_c \rightarrow J/\psi(\mu^+\mu^-)\ell^+X$ [1], it opened new avenues for experimental studies. With the LHCb experiment expected to produce about 5×10^{10} B_c mesons annually [2], precision measurements of its decay properties are now feasible. Unlike other heavy mesons, B_c decays exclusively via weak interactions, as strong and electromagnetic annihilation channels are forbidden. This unique feature results in a rich spectrum of decay modes, whose systematic study provides critical insights into weak interaction dynamics within the Standard Model and potential signatures of New Physics.

Rare transitions such as $b \rightarrow s\ell^+\ell^-$ and $b \rightarrow d\ell^+\ell^-$ are key probes of New Physics (NP) in heavy-flavor phenomenology. As Flavor-Changing Neutral Current (FCNC) processes, they are forbidden at tree level in the Standard Model (SM) and occur only through loop diagrams, primarily via Z - and photon-penguin contributions and W^+W^- box diagrams. Their sensitivity to short-distance effects makes them powerful tools for NP searches. Experimental studies began with $B \rightarrow K^{(*)}\ell^+\ell^-$ decays, first observed by CDF in 1998 [3], and have since been extensively measured by BELLE [4–9], BABAR [10–12], CMS [13], and LHCb [14–18], driving intense theoretical and experimental interest.

In recent works, we have analyzed semileptonic, nonleptonic, and rare decay modes of the B_c meson to S - and P -wave charmonium states [19], as well as to $D^{(*)}$ meson final states [20]. Building on this foundation, the present study focuses on the rare channels $B_c^- \rightarrow D_s^{(*)-}\ell^+\ell^-$ and $B_c^- \rightarrow D_s^{(*)-}\nu\bar{\nu}$, ($\ell = e, \mu, \tau$). These modes are sensitive to short-distance electroweak dynamics through penguin and box diagrams, analogous to $b \rightarrow s(d)$ transitions, but in a heavy-heavy quark system. Their study provides complementary information to the well-explored $b \rightarrow s\ell^+\ell^-$ transitions and offers an additional probe of lepton flavor universality (LFU). Our aim is to extract the q^2 -dependence of the $B_c \rightarrow D_s^*$ form factors using suitable parametrization methods, and subsequently to present predictions for the branching ratios for different lepton modes. We also perform a comprehensive angular analysis, including observables such as the forward–backward asymmetry, the longitudinal and transverse polarization fractions of the D_s^* meson, as well as a set of form-factor–independent clean observables within the SM framework.

Comparing observables in $B_c \rightarrow D_s^{(*)}$ and $B_c \rightarrow D^{(*)}$ decays [20] provides a powerful test of SU(3)-flavor symmetry and its breaking. Such comparisons are not merely academic, they are essential for understanding nonperturbative QCD effects that govern heavy meson dynamics. SU(3) breaking directly impacts hadronic form factors and wave functions, which are critical inputs for precise theoretical predictions. Constraining these effects improves the reliability of SM calculations and enhances sensitivity to potential New Physics contributions. With the anticipated large B_c sample at LHCb, these rare channels offer an unprecedented opportunity for high-precision measurements, making them a key probe for both SM validation and NP searches.

The contents of the paper are organised as follows: In section 2 we describe analytic expressions of the various physical observables we intend to predict and analyze in this work, along-with brief discussions on the relevant form factors in modified pQCD framework. In addition we also discuss the form of the LCDAs of the participating mesons. In section 3 we

extract the LCDA shape parameters of the participating mesons, and present predictions of the relevant form factors at $q^2 = 0$, calculated using the extracted parameters as inputs. In section 4 we extract information of $B_c \rightarrow D_s^*$ form factors over the full physical q^2 region, using some suitable symmetry relations and appropriate form factor parametrization. In section 5, we present our prediction of some physical observable, involving branching ratios and a number of angular observables along-with observables like forward backward asymmetry and longitudinal and transverse polarization fractions. Finally in section 6 we briefly summarize our work.

2 Theoretical Background

The very first thing to be clearly addressed is the theoretical background for the various aspects of the analysis in this work, particularly the physical observables. This section introduces the readers with discussions and explicit analytic expressions for the same. In subsection 2.1, we briefly introduce the physical observables we intend to predict in this work. In subsection 2.2 we discuss the form factor definitions in pQCD, and finally in subsection 2.3 we discuss the distribution amplitudes of the mesons participating in the processes studied in this work.

2.1 Physical Observables

In this subsection we briefly discuss about the various physical observables that we will be predicting in this work.

2.1.1 Decay widths and branching fractions

Contrary to the $B_c \rightarrow D^{(*)}$ modes, where both charged-current and neutral-current processes are allowed, the semileptonic charged-current channel is forbidden in the $B_c \rightarrow D_s^{(*)}$ modes. This is because in SM, the charged-current interaction couples the b quark only to c or u , and therefore cannot produce the $\bar{c}s$ configuration required to form a $D_s^{(*)}$ meson, resulting in tree-level $B_c^- \rightarrow D_s^{(*)-} \ell^- \bar{\nu}_\ell$ modes being forbidden. Consequently, for the $B_c \rightarrow D_s^{(*)}$ transitions, only the rare FCNC processes $b \rightarrow s \ell^+ \ell^-$ and $b \rightarrow s \nu \bar{\nu}$ are allowed and arise at loop level via penguin and box diagrams.

- For the decay mode $B_c^- \rightarrow D_s^{(*)-} \ell^+ \ell^-$ governed by $b \rightarrow s$ quark level transition, and shown in Figs 1 and 2. The most general effective Hamiltonian representing the above transition can be written as [21]

$$\mathcal{H}_{eff} = -\frac{4G_F}{\sqrt{2}} (\lambda_t \mathcal{H}_{eff}^t + \lambda_u \mathcal{H}_{eff}^u), \quad (2.1)$$

where $\lambda_i = V_{ib} V_{is}^*$ represents the CKM combination, and

$$H_{eff}^t = C_1 O_1^c + C_2 O_2^c + \sum_{i=3}^6 C_i O_i + \sum_{i=7}^{10} (C_i O_i + C'_i O'_i), \quad (2.2)$$

and

$$H_{eff}^u = C_1 (O_1^c - O_1^u) + C_2 (O_2^c - O_2^u), \quad (2.3)$$

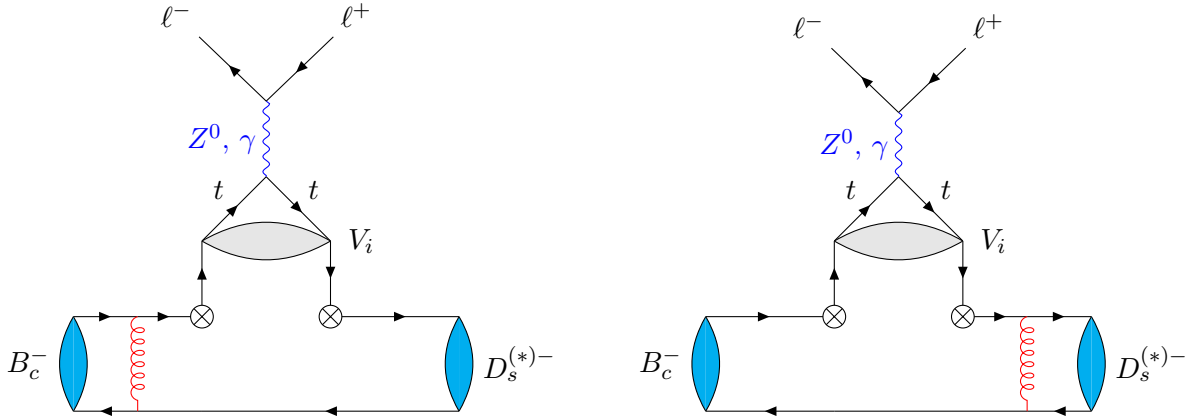


Figure 1: Z^0 and γ penguin diagrams in effective theory for $B_c^- \rightarrow D_s^{(*)-} \ell^+ \ell^-$ channel with $\ell = (e, \mu, \tau)$. V_i denotes the intermediate resonance states $\rho, \omega, \phi, J/\psi$ and $\psi(2S)$.

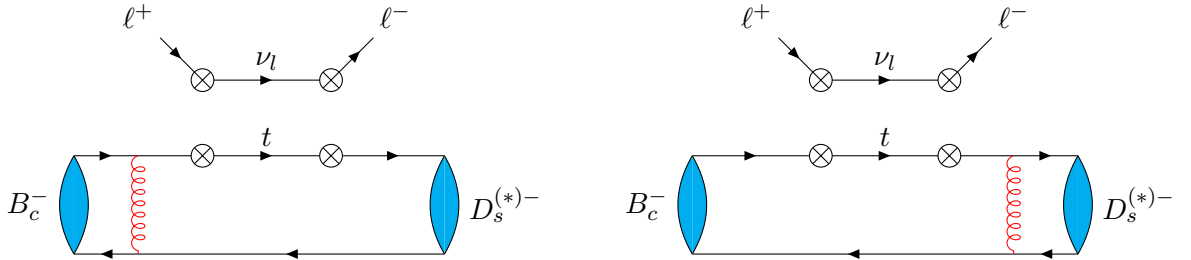


Figure 2: $W^+ W^-$ box diagrams in effective theory for $B_c^- \rightarrow D_s^{(*)-} \ell^+ \ell^-$ channel with $\ell = (e, \mu, \tau)$.

in the SM framework, $O_i \equiv O_i(\mu)$ represent the four Fermi operators, $C_i \equiv C_i(\mu)$ represent the corresponding Wilson coefficients, and μ being the re-normalization scale. The operators $O_{1,2}^{c,u}$ are the current-current operators, O_{3-6} the QCD penguin operators, $O_{7,8}$ the electromagnetic and chromomagnetic operators, and $O_{9,10}$ the semileptonic operators respectively. The expressions for the decay width are pretty much complicated and involved to be mentioned here. Hence, we refrain from discussing it in detail in this work and refer the readers to the references [22, 23] for their convenience.

- For the decay mode $B_c^- \rightarrow D_s^{*-} \nu \bar{\nu}$ the effective Hamiltonian is

$$\mathcal{H}_{eff}^{b \rightarrow s \nu \bar{\nu}} = \frac{G_F}{\sqrt{2}} \frac{\alpha_{EM}}{2\pi \sin^2(\theta_W)} V_{tb} V_{ts}^* \eta_X X(x_t) [\bar{s} \gamma^\mu (1 - \gamma_5) b] [\bar{\nu} \gamma_\mu (1 - \gamma_5) \nu], \quad (2.4)$$

where θ_W is the Weinberg angle with $\sin^2(\theta_W) = 0.231$. V_{tb} and V_{ts} are the CKM matrix elements. The function $X(x_t)$ has been taken from [24], and $\eta_X \approx 1$ represents

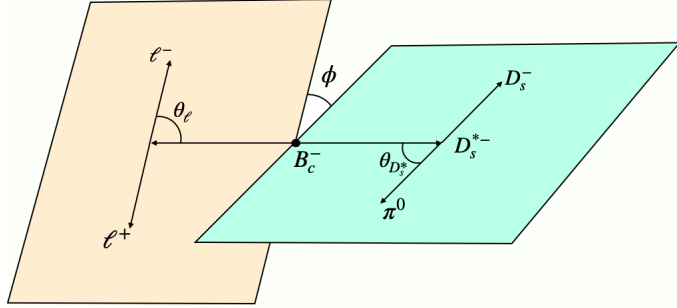


Figure 3: Kinematics of $B_c^- \rightarrow D_s^{*-} (\rightarrow D_s^- \pi^0) \ell^+ \ell^-$ four body decay.

the QCD correction factor. The differential decay width is expressed as [23, 25, 26]

$$\begin{aligned}
 \frac{d\Gamma(B_c \rightarrow D_s^* \nu \bar{\nu})}{dq^2} = & \frac{G_F^2 \alpha_{EM}^2}{2^{10} \pi^5 m_{B_c}^3} \cdot \left| \frac{X(x_t)}{\sin^2(\theta_W)} \right|^2 \cdot \eta_X^2 \cdot |V_{tb} V_{ts}^*|^2 \sqrt{\lambda(q^2)} \left\{ 8\lambda(q^2) q^2 \frac{V(q^2)^2}{(m_{B_c} + m_{D_s^*})^2} \right. \\
 & + \frac{\lambda(q^2)^2}{m_{D_s^*}^2} \cdot \frac{A_2(q^2)^2}{(m_{B_c} + m_{D_s^*})^2} + \frac{1}{m_{D_s^*}^2} (m_{B_c} + m_{D_s^*})^2 (\lambda(q^2) + 12m_{D_s^*}^2 q^2) \cdot A_1(q^2)^2 \\
 & \left. - \frac{2\lambda(q^2)}{m_{D_s^*}^2} (m_{B_c}^2 - m_{D_s^*}^2 - q^2) \cdot \text{Re}[A_1(q^2)^* A_2(q^2)] \right\}, \tag{2.5}
 \end{aligned}$$

where $\lambda(q^2)$, the phase space factor is expressed as

$$\lambda(q^2) = (m_{B_c}^2 + m_{D_s^*}^2 - q^2)^2 - 4m_{B_c}^2 m_{D_s^*}^2. \tag{2.6}$$

2.1.2 Angular analysis of rare $B_c^- \rightarrow D_s^{*-} \ell^+ \ell^-$ channel

Apart from the branching fractions, there are a number of other observables that are important in the present scenario of phenomenology. These primarily involve the angular observables, and a number of observables derived from them. These observables, being derived from $b \rightarrow s \ell^+ \ell^-$ transitions and governed via FCNC, are forbidden at tree-level in the SM and are sensitive to loop-level contributions, like the penguin and box diagrams shown in figures 1 and 2, thus making these channels interesting as probes to look for possible NP scenarios. With the effective Hamiltonian in eq. 2.1, a full angular decay rate distribution of $B_c^- \rightarrow D_s^{*-} (\rightarrow D_s^- \pi^0) \ell^+ \ell^-$ can be obtained, and can be expressed as

$$\frac{d^4\Gamma}{dq^2 d\cos\theta_{D_s^*} d\cos\theta_\ell d\phi} = \frac{9}{32\pi} \sum_i I_i(q^2) f_i(\theta_{D_s^*}, \theta_\ell, \phi), \tag{2.7}$$

with the angles $\theta_{D_s^*}$, θ_ℓ and ϕ has been shown in figure, where

- $\theta_{D_s^*}$ denotes the angle made by π^0 in the centre of mass system of D_s^- and π^0 with respect to the direction of flight of D_s^{*-} ,
- θ_ℓ denotes the angle made by ℓ^- in the centre of mass system of ℓ^+ and ℓ^- with respect to the direction of flight of the lepton pair, and

Angular Observables	$f_i(\theta_{D_s^*}, \theta_\ell, \phi)$	Angular Observables	$f_i(\theta_{D_s^*}, \theta_\ell, \phi)$
$I_{1s}(q^2)$	$\sin^2 \theta_{D_s^*}$	$I_5(q^2)$	$\sin 2\theta_{D_s^*} \sin \theta_\ell \cos \phi$
$I_{1c}(q^2)$	$\cos^2 \theta_{D_s^*}$	$I_{6s}(q^2)$	$\sin^2 \theta_{D_s^*} \cos \theta_\ell$
$I_{2s}(q^2)$	$\sin^2 \theta_{D_s^*} \cos 2\theta_\ell$	$I_7(q^2)$	$\sin 2\theta_{D_s^*} \sin \theta_\ell \sin \phi$
$I_{2c}(q^2)$	$\cos^2 \theta_{D_s^*} \cos 2\theta_\ell$	$I_8(q^2)$	$\sin 2\theta_{D_s^*} \sin 2\theta_\ell \sin \phi$
$I_3(q^2)$	$\sin^2 \theta_{D_s^*} \sin^2 \theta_\ell \cos 2\phi$	$I_9(q^2)$	$\sin^2 \theta_{D_s^*} \sin^2 \theta_\ell \sin 2\phi$
$I_4(q^2)$	$\sin 2\theta_{D_s^*} \sin 2\theta_\ell \cos \phi$		

Table 1: Expressions for $f_i(\theta_{D_s^*}, \theta_\ell, \phi)$. The corresponding angular coefficients are also mentioned the detailed mathematical expressions of which are given in the text.

- ϕ denotes the angle between the decay planes formed by the $(D_s^- \pi^0)$ and (ℓ^+, ℓ^-) pairs.

The $f_i(\theta_{D_s^*}, \theta_\ell, \phi)$ s are the functions which encode all the necessary angular information. Their forms are shown in table 1. The detailed mathematical expressions of the angular coefficients $I_i(q^2)$, which can be expressed in terms of various transversity amplitudes, are as given below:

$$\begin{aligned}
I_{1s} &= \left(\frac{3}{4} - \hat{m}_\ell^2 \right) \left(|\mathcal{A}_\parallel^L|^2 + |\mathcal{A}_\perp^L|^2 + |\mathcal{A}_\parallel^R|^2 + |\mathcal{A}_\perp^R|^2 \right) + 4\hat{m}_\ell^2 \text{Re} \left[\mathcal{A}_\perp^L \mathcal{A}_\perp^{L*} + \mathcal{A}_\parallel^L \mathcal{A}_\parallel^{R*} \right], \\
I_{1c} &= |\mathcal{A}_0^L|^2 + |\mathcal{A}_0^R|^2 + 4\hat{m}_\ell^2 (|\mathcal{A}_t|^2 + 2\text{Re}[\mathcal{A}_0^L \mathcal{A}_0^{R*}]), \\
I_{2s} &= \beta_\ell^2 \frac{|\mathcal{A}_\parallel^L|^2 + |\mathcal{A}_\parallel^R|^2 + |\mathcal{A}_\perp^L|^2 + |\mathcal{A}_\perp^R|^2}{4}, \\
I_{2c} &= -\beta_\ell^2 (|\mathcal{A}_0^L|^2 + |\mathcal{A}_0^R|^2), \\
I_3 &= \beta_\ell^2 \frac{|\mathcal{A}_\perp^L|^2 + |\mathcal{A}_\perp^R|^2 - |\mathcal{A}_\parallel^L|^2 - |\mathcal{A}_\parallel^R|^2}{2}, \\
I_4 &= \beta_\ell^2 \frac{\text{Re} \left[\mathcal{A}_0^L \mathcal{A}_\parallel^{L*} + \mathcal{A}_0^R \mathcal{A}_\parallel^{R*} \right]}{\sqrt{2}}, \\
I_5 &= \sqrt{2} \beta_\ell \text{Re} \left[\mathcal{A}_0^L \mathcal{A}_\perp^{L*} - \mathcal{A}_0^R \mathcal{A}_\perp^{R*} \right], \\
I_{6s} &= 2\beta_\ell \text{Re} \left[\mathcal{A}_\parallel^L \mathcal{A}_\perp^{L*} - \mathcal{A}_\parallel^R \mathcal{A}_\perp^{R*} \right], \\
I_7 &= \sqrt{2} \beta_\ell \text{Im} \left[\mathcal{A}_0^L \mathcal{A}_\parallel^{L*} - \mathcal{A}_0^R \mathcal{A}_\parallel^{R*} \right], \\
I_8 &= \beta_\ell^2 \frac{\text{Im} \left[\mathcal{A}_0^L \mathcal{A}_\perp^{L*} + \mathcal{A}_0^R \mathcal{A}_\perp^{R*} \right]}{\sqrt{2}}, \\
I_9 &= \beta_\ell^2 \text{Im} \left[\mathcal{A}_\parallel^L \mathcal{A}_\perp^L - \mathcal{A}_\parallel^R \mathcal{A}_\perp^R \right].
\end{aligned} \tag{2.8}$$

All these transversity amplitudes can further be expressed in terms of Wilson Coefficients $C_{7,9}^{eff}(\mu)$ and the form factors $A_{0,1,2}(q^2)$, $V(q^2)$ and $T_{1,2,3}(q^2)$, respectively. We have pre-

sented the detailed mathematical expressions of all these transversity amplitudes and other related information in appendix A.

The observables I_i s are hard to extract directly in experiments unless the B_c meson is tagged. Experimental measurements are often done with no distinction between B_c^+ or B_c^- . Therefore, it is more preferable to define a set of CP averaged observables, which are more easily measurable. For this, we define differential decay width of the CP conjugate decay mode $B_c^+ \rightarrow D_s^{*+} (\rightarrow D_s^+ \pi^0) \ell^+ \ell^-$ as

$$\frac{d^4\bar{\Gamma}}{dq^2 d\cos\theta_{D_s^*} d\cos\theta_\ell d\phi} = \frac{9}{32\pi} \sum_i \bar{I}_i(q^2) f_i(\theta_{D_s^*}, \theta_\ell, \phi), \quad (2.9)$$

where $f_i(\theta_{D_s^*}, \theta_\ell, \phi)$ has the same functional form as in table 1. The angular observables \bar{I}_i can be obtained from I_i by the replacements

$$\begin{aligned} I_{1s,1c,2s,2c,3,4,7} &\rightarrow \bar{I}_{1s,1c,2s,2c,3,4,7}, \\ I_{5,6s,8,9} &\rightarrow -\bar{I}_{5,6s,8,9}. \end{aligned} \quad (2.10)$$

This happens because for the CP conjugate mode, roles of ℓ^- and ℓ^+ get interchanged along with momentum flips, and handedness of decay planes which flip under parity, leading to

$$\theta_\ell \rightarrow \pi - \theta_\ell, \quad \phi \rightarrow -\phi. \quad (2.11)$$

With these we can define a set of CP averaged observables S_i and CP violating observables A_i defined by

$$S_i = \frac{I_i + \bar{I}_i}{d(\Gamma + \bar{\Gamma})/dq^2}, \quad A_i = \frac{I_i - \bar{I}_i}{d(\Gamma + \bar{\Gamma})/dq^2}, \quad (2.12)$$

where the observables have been normalized by the CP averaged differential decay width in order to reduce the form factor uncertainties. In addition, there are a number of physical observables that can be derived from the above observables.

- Integrating the differential decay width mentioned before over the angles $\theta_\ell \in [0, \pi]$, $\theta_{D_s^*} \in [0, \pi]$ and $\phi \in [0, 2\pi]$ the CP averaged differential decay width for $B_c^- \rightarrow D_s^{*-} (\rightarrow D_s^- \pi^0) \ell^+ \ell^-$ can be expressed as

$$\frac{d\Gamma_{CPavg}}{dq^2} = \frac{1}{2} \left(\frac{d\Gamma}{dq^2} + \frac{d\bar{\Gamma}}{dq^2} \right) = \frac{1}{4} (3I_{1c} + 6I_{1s} - I_{2c} - 2I_{2s}), \quad (2.13)$$

- the CP averaged lepton forward backward asymmetry expressed as

$$A_{FB} = \frac{3}{4} S_{6s}, \quad (2.14)$$

- The longitudinal and transverse polarization fractions of the D_s^* meson can be expressed as

$$\begin{aligned} F_L &= \frac{1}{4} (3S_{1c} - S_{2c}), \\ F_T &= \frac{1}{2} (3S_{1s} - S_{2s}), \end{aligned} \quad (2.15)$$

respectively,

- and clean angular observables $P_{1,2,3}$ and $P'_{4,5,6,8}$ expressed as [27, 28]

$$\begin{aligned}
P_1 &= \frac{S_3}{2S_{2s}}, & P'_4 &= \frac{S_4}{\sqrt{S_{1c}S_{2s}}}, \\
P_2 &= \frac{\beta_l S_{6s}}{8S_{2s}}, & P'_5 &= \frac{\beta_l S_5}{2\sqrt{S_{1c}S_{2s}}}, \\
P_3 &= -\frac{S_9}{4S_{2s}}, & P'_6 &= -\frac{\beta_l S_7}{2\sqrt{S_{1c}S_{2s}}}, \\
& & P'_8 &= -\frac{S_8}{\sqrt{S_{1c}S_{2s}}}.
\end{aligned} \tag{2.16}$$

2.2 Form Factors

In the previous subsection and in the appendix, we have mentioned that the transversity amplitudes are dependent on the QCD form factors. These form factors are functions that parametrize the hadronic matrix elements governing the B_c meson decays, and encode the QCD dynamics of the transition. Depending on the final state meson, whether it is pseudo-scalar or vector meson the transition matrix elements can be parametrized as

$$\begin{aligned}
\langle D_s(P_2) | \bar{q}(0) \gamma_\mu b(0) | B_{(c)}(P_1) \rangle &= \left[(P_1 + P_2)_\mu - \frac{M^2 - m^2}{q^2} q_\mu \right] F_+(q^2) \\
&\quad + \left[\frac{M^2 - m^2}{q^2} q_\mu \right] F_0(q^2),
\end{aligned} \tag{2.17}$$

for B_c meson decaying into D_s meson, governed by a vector current. For calculations in pQCD, however, it is much more convenient to express the form factors in terms of two auxillary form factors $f_1(q^2)$ and $f_2(q^2)$ defined as

$$\langle D(P_2) | \bar{q}(0) \gamma_\mu b(0) | B_{(c)}(P_1) \rangle = f_1(q^2) P_{1\mu} + f_2(q^2) P_{2\mu}, \tag{2.18}$$

and are related to $F_+(q^2)$ and $F_0(q^2)$ as

$$\begin{aligned}
F_+(q^2) &= \frac{1}{2} [f_1(q^2) + f_2(q^2)], \\
F_0(q^2) &= \frac{1}{2} f_1(q^2) \left[1 + \frac{q^2}{M^2 - m^2} \right] + \frac{1}{2} f_2(q^2) \left[1 - \frac{q^2}{M^2 - m^2} \right].
\end{aligned} \tag{2.19}$$

Next, for B_c meson decaying into D_s^* meson, the matrix element can be parametrized as

$$\langle D_s^*(P_2) | \bar{q}(0) \gamma_\mu b(0) | B_{(c)}(P_1) \rangle = \epsilon_{\mu\nu\alpha\beta} \epsilon^{\nu*} P_1^\alpha P_2^\beta \frac{2 \cdot V q^2}{M + m}, \tag{2.20}$$

and

$$\begin{aligned}
\langle D_s^*(P_2) | \bar{q}(0) \gamma_\mu \gamma_5 b(0) | B_{(c)}(P_1) \rangle &= i \left[\epsilon_\mu^* - \frac{\epsilon^* \cdot q}{q^2} q_\mu \right] (M + m) A_1(q^2) \\
&\quad - i \left[(P_1 - P_2)_\mu - \frac{M^2 - m^2}{q^2} q_\mu \right] (\epsilon^* \cdot q) \frac{A_2(q^2)}{M + m} \\
&\quad + i \left[\frac{2m(\epsilon^* \cdot q)}{q^2} q_\mu \right] A_0(q^2),
\end{aligned} \tag{2.21}$$

where the transition is governed by vector and axial-vector currents. In addition to the above, we also have the transition matrix elements governed by a tensor current as

$$\langle D_s(P_2) | \bar{q}(0) \sigma_{\mu\nu} b(0) | B_c(P_1) \rangle = i [P_{2\mu} q_\nu - q_\mu P_{2\nu}] \frac{2F_T(q^2)}{M + m}, \quad (2.22)$$

and

$$\begin{aligned} \langle D_s^*(P_2) | \bar{q}(0) \sigma_{\mu\nu} q^\nu (1 + \gamma_5) b(0) | B_c(P_1) \rangle &= i \epsilon_{\mu\nu\alpha\beta} \epsilon^{*\nu} P_1^\alpha P_2^\beta 2T_1(q^2) \\ &+ [\epsilon_\mu^*(M^2 - m^2) - (\epsilon^* \cdot q)(P_1 + P_2)_\mu] T_2(q^2) \\ &+ (\epsilon^* \cdot q) \left[q_\mu - \frac{q^2}{M^2 - m^2} (P_1 + P_2)_\mu \right] T_3(q^2). \end{aligned} \quad (2.23)$$

where $q^\mu = (P_1 - P_2)^\mu$ is the momentum transferred to the lepton part. P_1 and P_2 are the momenta carried by the initial and final state mesons and are expressed as

$$P_1 = \frac{M}{\sqrt{2}}(1, 1, 0_\perp), \quad P_2 = \frac{M}{\sqrt{2}}(r\eta^+, r\eta^-, 0_\perp), \quad (2.24)$$

respectively, in the light cone coordinate system, with $r = m/M$ and $\eta^\pm = \eta \pm \sqrt{\eta^2 - 1}$. The term η is expressed as

$$\eta = \frac{1 + r^2}{2r} - \frac{q^2}{2rM^2}. \quad (2.25)$$

Momenta of the spectator quarks in the initial and final state mesons can be expressed as

$$k_1 = \left(x_1 \frac{M}{\sqrt{2}}, x_1 \frac{M}{\sqrt{2}}, k_{1\perp} \right), \quad k_2 = \left(x_2 \frac{M}{\sqrt{2}} r\eta^+, x_2 \frac{M}{\sqrt{2}} r\eta^-, k_{2\perp} \right), \quad (2.26)$$

with x_1 and x_2 being the fraction of the total momentum carried by respective quarks, and M and m being the masses of initial and final state mesons respectively. A point to be noted is that these form factors are not independent, but are connected by some constraints arising specifically at $q^2 = 0$ in order to cancel the poles that appear at maximum recoil. These constraints go as

$$\begin{aligned} F_+(0) &= F_+(0), \\ 2rA_0(0) &= (1 + r)A_1(0) - (1 - r)A_2(0), \\ T_1(0) &= T_2(0). \end{aligned} \quad (2.27)$$

Form factors calculated in PQCD framework: The form factors defined above are the quantities that we intend to find out first. In pQCD framework [29], the form factors are expressed as a convolution of distribution amplitudes of the participating mesons, which encode the non-perturbative contributions and is process independent, a hard kernel, which encodes perturbative contributions and is process dependent, and an exponential term known as the Sudakov factor that reinforces the applicability of pQCD by suppressing the long distance contributions. They are expressed as

$$F_i \propto \phi_{B_{s,c}(x,b)} \otimes H(x, t) \otimes \phi_M(x, b) \otimes \exp[-S(P, b)], \quad (2.28)$$

where ϕ , $H(x, t)$ and $S(P, b)$ represent the distribution amplitudes of the participating mesons, hard kernel of the process and Sudakov factor respectively.

- The hard kernel describes the probability amplitude for a hard scattering event where the active quark from the B_s or B_c meson transfers momentum to either the spectator or the active quark of the final state meson, via a hard gluon exchange. It represents the short-distance interactions and is calculated perturbatively. We have presented the explicit expressions for the hard kernels used in this work in appendix C.
- As has been discussed in [29] for $B \rightarrow \pi$ form factor and in [30] for $B \rightarrow D^{(*)}$ form factors, they generate two kinds of double logarithmic enhancements, that must be resummed for the perturbative framework to remain valid.

- Threshold logarithms of the form $\ln^2(1 - x)$ or $\ln^2(x)$ that appear when the parton momentum fractions approach the end-point region, i.e., $x \rightarrow 0$ or $x \rightarrow 1$ [31]. These are resummed through the threshold resummation factor, expressed as

$$S_t(x) = \frac{2^{1+2c}\Gamma(\frac{3}{2} + c)}{\sqrt{\pi}\Gamma(1 + c)} [x(1 - x)]^c, \quad (2.29)$$

with $c = 0.3$ and suppresses contributions at the end-point regions, thereby preventing the resulting divergences.

- Transverse logarithms of the form $\ln^2(Pb)$, b being the impact parameter, and is Fourier conjugate to the transverse momentum k_T . When $b \rightarrow \infty$ or $k_T \rightarrow 0$, the double logarithm becomes large, signifying the uncontrollable growth of soft gluon contributions, leading to the form factors becoming divergent or unstable, making the perturbative theory unreliable. To regulate this behavior, these transverse logarithms are resummed to all orders, resulting in the Sudakov factor, which suppresses the contributions from large transverse separations and ensures the reliability of the pQCD calculation, and has the form as

$$s(Q, b) = \int_{1/b}^Q \frac{d\mu}{\mu} \left[\ln \left(\frac{Q}{\mu} \right) A(\alpha_s(\mu)) + B(\alpha_s(\mu)) \right], \quad (2.30)$$

for decay modes of heavy light meson, with $A(\alpha_s(\mu))$ and $B(\alpha_s(\mu))$ being the anomalous dimensions to two loops and one loop respectively, with their explicit expressions being taken from [29].

The B_c meson, being a heavy-heavy bound system, involves multiple scales, making resummation of such systems much more complicated compared to that for $B_{(s)}$ meson decays. However, taking the limit $m_b \rightarrow \infty$, but keeping m_c finite, the B_c meson can be treated as a heavy-light system and analysis of the decays can be carried out in conventional pQCD approach for B meson decays [30]. This approximation, first introduced in [32], modifies the Sudakov factors, thus leading to a modified pQCD formalism. The Sudakov factor thus derived has the form

$$\begin{aligned} s_c(Q, b) &= s(Q, b) - s(m_c, b), \\ &= \int_{m_c}^Q \frac{d\mu}{\mu} \left[\int_{1/b}^{\mu} \frac{d\bar{\mu}}{\bar{\mu}} A(\alpha_s(\bar{\mu})) + B(\alpha_s(\bar{\mu})) \right]. \end{aligned} \quad (2.31)$$

However it is to be noted that in case of B_s mesons, this modified pQCD framework is not necessary. This is because, unlike B_c mesons, the B_s meson is formed by the b and s quarks, the former being a heavy quark and the latter a light quark. Thus, the analysis of B_s mesons can be carried on using the conventional pQCD approach [30], and the introduction of a finite charm quark mass scale is not required in this case. We present explicit expressions of the form factors, along with appropriate references in appendix B.

2.3 Light Cone Distribution amplitudes

In the last subsection, we discussed that the form factors in pQCD have distribution amplitude of the participating mesons in the convolution. In this subsection, we briefly discuss the form of the distribution amplitudes used in this work. Light cone distribution amplitudes (LCDAs) encode how the momentum of a fast-moving hadron is distributed among the constituent quarks along the light cone direction. These serve as crucial non-perturbative inputs to the form factor expressions in pQCD, and their shape offers a degree of flexibility to obtain predictions of the form factors, by constraining them through model-independent techniques. For this work, we will be discussing the LCDAs of the B_s , B_c and $D_s^{(*)}$ mesons. Reason for considering the B_s meson LCDA will be explained in the following section.

- For B_s meson, the wavefunction has the form as

$$\Phi_{B_s}(p, x) = \frac{i}{\sqrt{2N_c}} \left(\not{p}_{B_s} + M \right) \gamma_5 \phi_{B_s}(x, b), \quad (2.32)$$

where $\phi_{B_s}(x, b)$ represents the B_s meson LCDA, which assumes an approximate Gaussian form as [30, 33]

$$\phi_{B_s}(x, b) = \frac{f_{B_s}}{2\sqrt{2N_c}} N_{B_s} x^2 (1-x)^2 \exp \left[-\frac{x^2 M^2}{2\omega_{B_s}^2} - \frac{1}{2} \omega_{B_s}^2 b^2 \right], \quad (2.33)$$

with $M = m_{B_s}$, ω_{B_s} the shape parameter defining the shape of the distribution amplitude, and N_{B_s} the normalization constant fixed by the relation

$$\int_0^1 \phi_{B_s}(x, b=0) dx = \frac{f_{B_s}}{2\sqrt{2N_c}}, \quad (2.34)$$

where f_{B_s} is the decay constant of B_s meson.

- For B_c meson, the wavefunction has the form as

$$\Phi_{B_c}(p, x) = \frac{i}{\sqrt{2N_c}} \left(\not{p}_{B_c} + M \right) \gamma_5 \phi_{B_c}(x, b), \quad (2.35)$$

where $M = m_{B_c}$ and $\phi_{B_c}(x, b)$ represents the B_c meson LCDA, which we consider to have an approximate Gaussian form as [32]

$$\phi_{B_c}(x, b) = \frac{f_{B_c}}{2\sqrt{2N_c}} N_{B_c} x (1-x) \exp \left[-\frac{(1-x)m_c^2 + xm_b^2}{8\omega_{B_c}^2 x(1-x)} \right] \exp[-2 \omega_{B_c}^2 x(1-x)b^2], \quad (2.36)$$

The normalization constant N_{B_c} is fixed by the relation

$$\int_0^1 \phi_{B_c}(x, b=0) dx = \frac{f_{B_c}}{2\sqrt{2N_c}}, \quad (2.37)$$

and the parameter b being the impact parameter, which is infact Fourier conjugate to the transverse momentum k_T , ω_{B_c} being the shape parameter of the B_c meson distribution amplitude and f_{B_c} the decay constant of B_c meson.

- For D_s and D_s^* mesons, the wavefunctions have the same form as in [34]

$$\begin{aligned} \Phi_{D_s}(p, x) &= \frac{i}{\sqrt{2N_c}} \gamma_5 (\not{p}_{D_s} + m) \phi_{D_s}(x, b), \\ \Phi_{D_s^*}(p, x) &= -\frac{i}{\sqrt{2N_c}} [\not{\epsilon}_L (\not{p}_{D_s^*} + m) \phi_{D_s^*}^L(x, b) + \not{\epsilon}_T (\not{p}_{D_s^*} + m) \phi_{D_s^*}^T(x, b)], \end{aligned} \quad (2.38)$$

where $m = m_{D_s^{(*)}}$, $\phi_{D_s}(x, b)$, $\phi_{D_s^*}^L(x, b)$ and $\phi_{D_s^*}^T(x, b)$ the LCDAs of respective mesons. In this work we consider these to have a simple polynomial form as [35]

$$\phi_{D_s^{(*)}}(x, b) = \frac{f_{D_s^{(*)}}}{2\sqrt{2N_c}} 6x(1-x) \left[1 + C_{D_s^{(*)}}(1-2x) \right] \cdot \exp \left[-\frac{\omega_{D_s^{(*)}}^2 b^2}{2} \right], \quad (2.39)$$

where $C_{D_s^{(*)}}$ and $\omega_{D_s^{(*)}}$ are parameters that control the shape of the corresponding distribution amplitudes. $\phi_{D_s^{(*)}}$ satisfies the normalization condition

$$\int_0^1 \phi_{D_s^{(*)}}(x, 0) dx = \frac{f_{D_s^{(*)}}}{2\sqrt{2N_c}}, \quad (2.40)$$

with $f_{D_s^{(*)}}$ being the decay constant of the respective meson.

In most existing studies on B_s and B_c decays in pQCD framework [26, 32, 34], the authors simply treat the shape parameters (ω_{B_s} , ω_{B_c} , etc.) as fixed numbers. They also restrict their use of Lattice QCD data to just the maximum momentum transfer (q_{\max}^2). Our work takes a different approach. Instead of fixing these values beforehand, we treat them as free parameters and find their best values by fitting them to the data. By analyzing the $B_c \rightarrow D_s$ and $B_s \rightarrow D_s^{(*)}$ channels together, we get a consistent set of parameters for everyone. This combined method also lets us see how the parameters are connected to each other (the correlation matrix), something we cannot infer if we analyze the channels separately. Understanding these connections is key to getting reliable error estimates for our final predictions.

3 Extraction of LCDA shape parameters and form factors at $q^2 = 0$

With all the theoretical pre-requisites discussed we now move onto extracting the shape parameters of LCDAs of the participating mesons. For the $B_c \rightarrow D_s$ mode, HPQCD [39] has obtained information of the form factors over full q^2 region using Bourrley-Caprini-Lellouch (BCL) [40] parametrization, through which we can conveniently obtain the relevant

Mass (GeV)	$m_{B_c} = 6.274$	$m_{B_s} = 5.367$
	$m_{D_s} = 1.969$	$m_{D_s^*} = 2.112$
	$m_e = 0.511 \times 10^{-3}$	$m_\mu = 0.105$
		$m_\tau = 1.776$
Decay constants (GeV)	$f_{B_c} = 0.427(6)$ [36]	$f_{B_s} = 0.229(5)$ [37]
	$f_{D_s} = 0.2480(25)$ [37]	$f_{D_s^*} = 0.2688(65)$ [37]
CKM matrix elements [38]	$ V_{cb} = 41.1(1.2) \times 10^{-3}$	
	$ V_{us} = 0.22431(85)$	$ V_{ub} = 3.82(20) \times 10^{-3}$
	$ V_{ts} = 41.5(9) \times 10^{-3}$	$ V_{tb} = 1.010(27)$
Lifetime (ps)	$\tau_{B_c} = 0.510(9)$ [38]	

Table 2: Values of input parameters used in this work.

form factors at $q^2 = 0$. Additionally, to better constrain the $D_s^{(*)}$ LCDA shape parameters, we consider the $B_s \rightarrow D_s^{(*)}$ modes, information of which has been supplied by HPQCD [41, 42]. In addition to the lattice inputs, we also use inputs of the respective form factors presented in the LCSR approach [43]. The numerical values of the form factor data for the first chi-square minimization are shown in table 3.

Finally, we construct a chi-square function with the shape parameters as free parameters, and then minimize it. The chi-square function has the form

$$\chi^2 = \sum_{i,j} (\mathcal{O}_i^{th} - \mathcal{O}_i^{data}) V_{ij}^{-1} (\mathcal{O}_j^{th} - \mathcal{O}_j^{data})^T + \chi^2_{nuis}, \quad (3.1)$$

where \mathcal{O}_i^{th} represents the pQCD expressions for form factors at $q^2 = 0$, \mathcal{O}_i^{data} represents the inputs on the corresponding form factors at $q^2 = 0$ and V_{ij} represents the covariance matrix between the inputs. χ^2_{nuis} represents the chi-square function constructed with the relevant nuisance parameters.

Decay Channel	Form Factors	Values at $q^2 = 0$		
		Lattice		LCSR
		Group	Value	
$B_s \rightarrow D_s$	$F_+(0)$	HPQCD	0.665(12)	0.708(153)
$B_s \rightarrow D_s^*$	$A_0(0)$		0.611(55)	0.731(187)
	$A_1(0)$	HPQCD	0.591(40)	0.633(143)
	$V(0)$		0.977(153)	0.735(176)
$B_c \rightarrow D_s$	$F_+(0)$	HPQCD	0.217(18)	-
	$F_T(0)$		0.299(54)	-

Table 3: Form factor data for $B_s \rightarrow D_s^{(*)}$ and $B_c \rightarrow D_s$ semileptonic channels at $q^2 = 0$.

Additionally, we take the charm and bottom quark masses, m_c and m_b , as the arithmetic averages of their values in the pole, \overline{MS} , and kinetic schemes. To ensure a scheme-independent and inclusive treatment of mass uncertainties, we assign relative errors of 25% for m_c and 10% for m_b , chosen to encompass the full range of variation across these schemes. The quark masses are presented in table 4.

Scheme	m_b (GeV)	m_c (GeV)
Pole mass	4.78	1.67
\overline{MS}	4.18	1.273
Kinetic	4.56	1.091
Average	4.506(451)	1.345(336)

Table 4: Values of m_b and m_c in three different schemes and their average value [38].

With these inputs, we can now construct the relevant chi-square function and then minimize it to extract the required shape parameters of the meson LCDAs, i.e. ω_{B_c} , $C_{D_s^{(*)}}$ and $\omega_{D_s^{(*)}}$ along with bottom and charm quark masses as nuisance parameters. Our current analysis already incorporates radiative corrections up to $\mathcal{O}(\alpha_s)$ and $\mathcal{O}(\alpha_s^2)$, following the calculations in Ref. [44] for B mesons and in [45] for B_c meson wave functions. The calculations are relevant for the $B_s \rightarrow P(V)$ and $B_c \rightarrow P(V)$ form factors within the PQCD framework. Furthermore, we emphasize that the pQCD form factors employed in this analysis incorporate only the leading-order (LO) contributions in the hard kernel, and the meson wave functions are defined within the leading-twist approximation.

Light-cone distribution amplitudes (LCDAs) describe how the momentum of a hadron is shared among its constituent partons when projected onto the light cone. In our analysis, we employ a QCD-inspired distribution amplitude, meaning that the longitudinal part of the light-cone wave function is constrained by principles of Quantum Chromodynamics (QCD), rather than being purely phenomenological as in the simple Gaussian ansatz.

A Gaussian ansatz is mathematically convenient but does not accurately represent QCD dynamics; in particular, it suppresses the endpoint regions $x \rightarrow 0$ and $x \rightarrow 1$ too strongly. QCD-inspired DAs avoid this issue because they incorporate information from QCD sum rules, lattice QCD, and the known perturbative-QCD asymptotic behavior. Consequently, they provide realistic endpoint behavior and a more accurate momentum-fraction dependence.

In our framework, the full light-cone wave function is written as the product of two components:

1. the longitudinal distribution amplitude, taken from a QCD-inspired model, and
2. a transverse-momentum profile, for which we use a scale-independent Gaussian function.

This approach preserves the simplicity of a Gaussian transverse profile while improving the physical accuracy of the longitudinal structure through QCD-based constraints.

In the light-cone formalism, the twist of an operator is defined as the difference between its mass dimension and its spin. The leading contribution arises from twist-2 operators, which correspond to the simplest quark–antiquark configuration and dominate the behavior at large momentum transfer. In this work, we restrict our attention to the leading-twist light-cone distribution amplitudes (LCDAs).

Higher-twist terms (twist-3, twist-4, etc.) originate from several sources, such as

- intrinsic transverse momentum of quarks,
- quark-gluon interactions,
- and more involved multi-parton correlations.

Although these contributions are formally suppressed by powers of Λ_{QCD}/m_Q , they may still play a significant role, especially at low and intermediate values of q^2 , where nonperturbative effects become more pronounced. Twist-3 amplitudes typically involve pseudoscalar and tensor components, while twist-4 terms incorporate explicit quark–gluon operator structures. Including these higher-twist effects introduces additional nonperturbative parameters but can enhance the precision and reliability of form-factor predictions.

However, in the present analysis we do not have sufficient input to reliably constrain all higher-twist contributions. To account for the possible impact of these missing effects, we introduce an additional theoretical uncertainty in the LCDA shape parameters and in the resulting form factors. Previous studies of $B \rightarrow \pi$ and $B \rightarrow \rho$ form factors within the pQCD framework (see Refs. [23, 46, 47]) show that next-to-leading-order (NLO) corrections to the hard kernel, together with higher-twist effects, can induce shifts of about 20–30% relative to leading-order (LO) predictions. Motivated by these findings, we conservatively assign a 30% uncertainty to our LO form factor predictions to cover the dominant theoretical uncertainties associated with neglected higher-order radiative corrections and higher-twist LCDA contributions.

This uncertainty is implemented through a multiplicative nuisance parameter, δ_{f_i} , which is constrained to lie within this range. Treating δ_{f_i} as a nuisance parameter during the minimization procedure ensures that its effect is consistently propagated into the final uncertainties of the extracted shape parameters.

When constructing the χ^2 function, we do not include the uncertainties of the meson decay constants in χ^2_{nuis} , since their errors are typically only at the level of 2–3% (see Table 2). Compared to the much larger theoretical uncertainties associated with the form factors, the impact of varying these decay constants on the fit results is negligible.

We present our estimates of the thus extracted parameters in table 5 along with the corresponding correlation matrix in table 23. Checking table 5 we see that $\chi^2_{\text{min}}/\text{DOF} < 1$, signifying that our fit is statistically good. We also see that our estimate of ω_{B_c} is in good agreement with our previously extracted value in [19, 20], thereby justifying its estimate through three independent analyses. Our estimates of shape parameters of B_s and $D_s^{(*)}$ mesons are also in good agreement with existing model-dependent estimates.

Taking these extracted parameters as inputs into the pQCD expressions of form factors, we can obtain predictions of form factors at $q^2 = 0$. We present our estimates, along with

Free Parameters		Nuisance Parameters	
Parameters	Fit Results	Parameters	Fit Results
ω_{B_c}	1.011(60) GeV	m_b	4.505(112) GeV
ω_{B_s}	0.493(31) GeV	m_c	1.330(64) GeV
C_{D_s}	0.496(66)	$\delta_{f_1}^{B_s \rightarrow D_s}$	-0.064(91)
$C_{D_s^*}$	0.505(44)	$\delta_{f_2}^{B_s \rightarrow D_s}$	0.002(100)
ω_{D_s}	0.101(11)	$\delta_{A_0}^{B_s \rightarrow D_s^*}$	-0.047(94)
$\omega_{D_s^*}$	0.099(14)	$\delta_{A_1}^{B_s \rightarrow D_s^*}$	-0.011(105)
		$\delta_V^{B_s \rightarrow D_s^*}$	-0.028(77)
		$\delta_{f_1}^{B_c \rightarrow D_s}$	-0.057(111)
		$\delta_{f_2}^{B_c \rightarrow D_s}$	-0.113(114)
		$\delta_{F_T}^{B_c \rightarrow D_s}$	0.053(92)
DOF	4		
χ^2_{min}/DOF	0.544		
p-Value	70.31%		

Table 5: Extracted values of LCDA parameters obtained by fitting pQCD form factors of $B_c \rightarrow D_s$ and $B_s \rightarrow D_s^{(*)}$ transitions with corresponding lattice and LCSR inputs at $q^2 = 0$.

comparisons with previous pQCD and other model-dependent predictions in table 6, and the corresponding correlation matrix in table 24. In these predictions, we have explicitly applied a 30% correction factor to account for uncertainties arising from loop-level corrections and next-to-leading-twist LCDAs. Furthermore, the errors associated with the decay constants have also been propagated independently to the final results.

Form Factors	This work	Previous PQCD[26]	CLFQM[48]
$A_0^{B_c \rightarrow D_s^*}(0)$	0.288(78)	0.21(4)	$0.17^{+0.01+0.01}_{-0.01-0.01}$
$A_1^{B_c \rightarrow D_s^*}(0)$	0.257(68)	0.23(4)	$0.14^{+0.01+0.02}_{-0.01-0.01}$
$A_2^{B_c \rightarrow D_s^*}(0)$	0.235(48)	0.25(5)	$0.12^{+0.01+0.02}_{-0.01-0.02}$
$V^{B_c \rightarrow D_s^*}(0)$	0.252(77)	0.33(6)	$0.23^{+0.02+0.03}_{-0.02-0.02}$
$T_1^{B_c \rightarrow D_s^*}(0)$	0.274(87)	0.28(6)	-
$T_2^{B_c \rightarrow D_s^*}(0)$	0.274(83)	0.28(6)	-
$T_3^{B_c \rightarrow D_s^*}(0)$	0.194(60)	0.27(6)	-

Table 6: Prediction of form factors of $B_c \rightarrow D_s^*$ transition at $q^2 = 0$ along with comparison with other predictions.

Revisiting the form factor expressions in Appendix B, we can see that the integrations

over b_1 and b_2 have been done up to a cut-off b_c . In this work, we have set it at around 90% of $1/\Lambda_{QCD}$. This has been done to keep our calculations well within the perturbative QCD region and to avoid them from including any non-perturbative contributions. Regarding the error estimates for each form factor in table 6, we observe that they are much larger than those of previous pQCD predictions. This is mainly due to the 30% uncertainty that we have propagated as systematic error. In addition, we have the parameters ω_{B_c} , $C_{D_s^{(*)}}$, $\omega_{D_s^{(*)}}$, m_b and m_c that also contribute to the total error. On the contrary, the predictions in ref. [26] have used model-dependent values of all these parameters, and no errors are considered in $C_{D_s^{(*)}}$ and $\omega_{D_s^{(*)}}$, only a 10% error has been introduced in ω_{B_c} .

4 Obtaining form factor information over full physical q^2 range

In the previous section, we had calculated the form factors at $q^2 = 0$. However, when it comes to prediction of physical observables, this is not enough, since, as we have seen in section 2, we need form factor information over full physical q^2 range for doing so. PQCD as a framework, is itself not enough since it is more reliable in the smaller q^2 region, i.e., near $q^2 = 0$. To overcome this limitation, we derive certain symmetry relations valid at high q^2 region to connect the $B_c \rightarrow D_s$ form factors, whose information we have, with $B_c \rightarrow D_s^*$ form factors, whose information we want to obtain. Following this, we adopt certain parametrization method to obtain information of $B_c \rightarrow D_s^*$ form factors over the full q^2 region. We divide this section into three subsections. In subsection 4.1 we derive the symmetry relations between the relevant form factors. In subsection 4.2 we extract necessary parameters, and in subsection 4.3 we perform the appropriate parametrization and obtain form factor information over the full physical q^2 region.

4.1 Connecting $B_c \rightarrow D_s^*$ with $B_c \rightarrow D_s$ form factors

In this subsection we briefly discuss about the relations connecting the $B_c \rightarrow D_s$ and $B_c \rightarrow D_s^*$ form factors. We use the Heavy-Quark-Effective-Theory (HQET) trace formalism, retaining both leading and subleading contributions in the heavy-quark limit. This allows us to express all the form factors by just two universal form factors.

Following the trace formalism developed in [49, 50], the weak matrix element in HQET for transitions with a generic Dirac bilinear Γ can be expressed as

$$\langle D_s^{(*)}(v, k) | \bar{q} \Gamma Q | B_c(v) \rangle = -\sqrt{Mm} \text{ Tr}[\bar{H}^{(\bar{c})} \Sigma(v, a_0 k) \Gamma H^{(c\bar{b})}], \quad (4.1)$$

with the initial state meson and the final state mesons carry four momenta $P_1 = Mv$ and $P_2 = mv + k$ respectively, with k being a small residual momentum. The B_c^+ and B_c^{*+} doublet comprising of two heavy quarks \bar{b} and c is represented by the effective field

$$H^{c\bar{b}} = \frac{1+\not{v}}{2} [B_c^{*\mu} \gamma_\mu - B_c \gamma_5] \frac{1-\not{v}}{2}, \quad (4.2)$$

and the D_s and D_s^* doublet with a single heavy quark c is represented by the effective fields

$$H^c = [D_s^{*\mu} \gamma_\mu - D_s \gamma_5] \frac{1-\not{v}}{2}. \quad (4.3)$$

The term $\Sigma(v, a_0 k)$ can be generalized in terms of two dimensionless functions as

$$\Sigma(v, a_0 k) = \Sigma_1 + \not{k} a_0 \Sigma_2, \quad (4.4)$$

with Σ_1 and Σ_2 being the universal form factors that encode the non-perturbative QCD dynamics of the light degrees of freedom. The function Σ_1 arises at leading order contribution to the HQET expansion of the matrix element and reflects the structure dictated by Heavy Quark Spin Symmetry (HQSS), which becomes exact in the infinite mass limit. The second function Σ_2 , however, captures the leading corrections to this symmetry. These corrections are associated with residual momentum k of $D_s^{(*)}$ meson, and introduce the $\mathcal{O}(1/m_Q)$ symmetry breaking effects. a_0 has the dimension of length and is typically the Bohr radius of the B_c meson. The a_0 factor suppresses Σ_2 compared to Σ_1 , thus making the symmetry breaking effects small. The weak matrix element for $B_c \rightarrow D_s$ transition is then obtained as

$$\langle D_s(v, k) | \bar{q} \gamma_\mu Q | B_c(v) \rangle = 2\sqrt{Mm} [\Sigma_1(w) v_\mu + a_0 \Sigma_2(w) k_\mu], \quad (4.5)$$

where the recoil parameter w is related is q^2 as

$$w = \frac{M^2 + m^2 - q^2}{2Mm}. \quad (4.6)$$

Following the same method, the $B_c \rightarrow D_s$ matrix element induced by the tensor current can be expressed as

$$\langle D_s(v) | \bar{q} \sigma_{\mu\nu} Q | B_c(v) \rangle = -2i\sqrt{Mm} a_0 \Sigma_2(w) (v_\mu k_\nu - v_\nu k_\mu), \quad (4.7)$$

and the $B_c \rightarrow D_s^*$ matrix elements induced by vector, axial-vector and tensor currents can be expressed as

$$\langle D_s^*(v, k, \epsilon) | \bar{q} \gamma_\mu Q | B_c(v) \rangle = 2\sqrt{Mm} \epsilon_{\mu\nu\alpha\beta} \epsilon^{*\nu} v^\alpha k^\beta a_0 \Sigma_2(w), \quad (4.8)$$

$$\begin{aligned} \langle D_s^*(v, \epsilon) | \bar{q} \gamma_\mu \gamma_5 Q | B_c(v) \rangle = 2i\sqrt{Mm} & \left[\epsilon_\mu^* (\Sigma_1(w) + v \cdot k a_0 \Sigma_2(w)) \right. \\ & \left. - \left(v_\mu - \frac{k_\mu}{m} \right) \epsilon^* \cdot k a_0 \Sigma_2(w) \right], \end{aligned} \quad (4.9)$$

$$\langle D_s^*(v, \epsilon) | \bar{q} \sigma_{\mu\nu} q^\nu Q | B_c(v) \rangle = 2i\sqrt{Mm} \epsilon_{\mu\nu\alpha\beta} \epsilon^{*\beta} [v^\alpha \Sigma_1(w) + k^\alpha a_0 \Sigma_2(w)] [(M - m)v^\nu - k^\nu], \quad (4.10)$$

and

$$\begin{aligned} \langle D_s^*(v, \epsilon) | \bar{q} \sigma_{\mu\nu} q^\nu \gamma_5 Q | B_c(v) \rangle = & 2\sqrt{Mm} \left[\epsilon_\mu^* (v_\nu \Sigma_1(w) + k_\nu a_0 \Sigma_2(w)) \right. \\ & \left. - \epsilon_\nu^* (v_\mu \Sigma_1(w) + k_\mu a_0 \Sigma_2(w)) \right] [(M - m)v^\nu - k^\nu], \end{aligned} \quad (4.11)$$

respectively. Matching these HQET matrix elements with the ones previously discussed in subsection 2.2 we can express all the full QCD form factors in terms of $\Sigma_1(w)$ and $\Sigma_2(w)$. For $B_c \rightarrow D_s$ form factors, we get the relations as

$$\begin{aligned} F_+(w) &= \sqrt{\frac{m}{M}} (\Sigma_1(w) + (M - m)a_0\Sigma_2(w)), \\ F_0(w) &= \frac{2\sqrt{Mm}}{M^2 - m^2} [(M - mw)\Sigma_1(w) + m(M + m)(w - 1)a_0\Sigma_2(w)], \\ F_T(w) &= \sqrt{\frac{m}{M}} (M + m)a_0\Sigma_2(w), \end{aligned} \quad (4.12)$$

and for the $B_c \rightarrow D_s^*$ form factors, we get the relations as

$$\begin{aligned} V(w) &= \sqrt{\frac{m}{M}} (M + m)a_0\Sigma_2(w), \\ A_0(w) &= \frac{2M\Sigma_1(w) + ((M - 2m)(2mw - M) + (2m^2 + M^2 - 2Mmw))a_0\Sigma_2(w)}{2\sqrt{Mm}}, \\ A_1(w) &= \frac{2\sqrt{Mm}}{M + m} (\Sigma_1(w) + m(w - 1)a_0\Sigma_2(w)), \\ A_2(w) &= \frac{\sqrt{Mm}(M - 2m)(M + m)a_0\Sigma_2(w)}{M^2}, \end{aligned} \quad (4.13)$$

for the vector and axial-vector form factors, and

$$\begin{aligned} T_1(w) &= \sqrt{\frac{m}{M}} [\Sigma_1(w) + (M - m)a_0\Sigma_2(w)], \\ T_2(w) &= \frac{2\sqrt{Mm}}{M^2 - m^2} [\Sigma_1(w)(M - mw) + (m(M + m)(w - 1))a_0\Sigma_2(w)], \\ T_3(w) &= \sqrt{\frac{m}{M}} [-\Sigma_1(w) + (M + m)a_0\Sigma_2(w)], \end{aligned} \quad (4.14)$$

for the tensor form factors. In all the calculations, since we have not neglected the symmetry breaking corrections, we have not neglected $v \cdot k$, and also have considered the contributions coming from k_μ/m . At this point we would like to re-iterate that these relations were presented in our earlier work [20]. However, we include a brief discussion here as well to make the present work self-contained and the notations easier to follow.

4.2 Extracting the universal functions Σ_1 and Σ_2

With expressions for the form factors in terms of soft functions Σ_1 and Σ_2 derived, we move onto extracting the shape of these functions in this subsection. These universal functions are well defined around q_{max}^2 , or near $w = 1$, where the initial and final meson states have the same velocities, thus making it possible to expand these functions into a Taylor series

around $w = 1$, enabling us to express them in a parametric form defined as

$$\begin{aligned}\Sigma_1(w) &= \Sigma_1(1) + \Sigma'_1(w-1) + \frac{1}{2}\Sigma''_1(w-1)^2, \\ a_0\Sigma_2(w) &= a_0\Sigma_2(1) + a_0\Sigma'_2(w-1) + \frac{1}{2}a_0\Sigma''_2(w-1)^2,\end{aligned}\tag{4.15}$$

where $\Sigma_1(1)$, Σ'_1 , Σ''_1 , $a_0\Sigma_2(1)$, $a_0\Sigma'_2$ and $a_0\Sigma''_2$ are the coefficients that control the shape of these functions.

To extract these coefficients, we construct a chi-square function with $B_c \rightarrow D_s$ lattice form factors at $w = 1.0$, 1.15 and 1.3 as inputs (refer to table 20) and their corresponding expressions presented in eqn.(4.12), and then minimize it. The thus extracted coefficients, along with the corresponding correlation matrix is presented in table 7.

Parameters	Our estimates	Correlation					
		$\Sigma_1(1)$	Σ'_1	Σ''_1	$a_0\Sigma_2(1)$ (GeV^{-1})	$a_0\Sigma'_2$ (GeV^{-1})	$a_0\Sigma''_2$ (GeV^{-1})
$\Sigma_1(1)$	0.860(12)	1.0	-0.551	0.357	0.104	-0.114	0.106
Σ'_1	-3.111(89)		1.0	-0.883	-0.372	0.298	-0.285
Σ''_1	8.645(420)			1.0	0.414	-0.450	0.460
$a_0\Sigma_2(1)$ (GeV^{-1})	0.444(12)				1.0	-0.861	-0.795
$a_0\Sigma'_2$ (GeV^{-1})	-1.577(83)					1.0	-0.985
$a_0\Sigma''_2$ (GeV^{-1})	4.244(278)						1.0
DOF	3						
χ^2/DOF	1.916						
p-Value	12.46%						

Table 7: Estimates of coefficients of Σ_1 and $a_0\Sigma_2$.

From table 7 we observe that estimates of $a_0\Sigma_2$ coefficients are about 50% suppressed compared to those for Σ_1 , signifying that the symmetry-breaking contributions to the matrix elements, although not zero, are significantly suppressed compared to the leading-order contribution. Using the coefficients in table 7 as inputs in eqn.(4.15), we can now obtain the w distribution of both Σ_1 and $a_0\Sigma_2$. We present the plots of these functions in figure 4. The error estimate is calculated by propagating the error estimates of HPQCD form factor inputs. Since this method is more reliable near $w = 1$, we confine our plots in the region $w \in (1, 1.3)$.

Additionally, for reference to the readers, in figure 5 we also present q^2 distribution of the $B_c \rightarrow D_s$ form factors F_+ , F_0 and F_T , using the extracted universal function parameters as inputs. The uncertainty in each form factor is controlled primarily by that of F_0 and F_T , which ranges between 1.5 and 3.0%. This results in the uncertainty in F_+ being tightly constrained relative to the input. Furthermore, we observe that the shapes are well-behaved and monotonically decreasing up to $q^2 \approx 11 \text{ GeV}^2$, which corresponds to $w \approx 1.3$. Below this point, the shape of the form factors rises abruptly, thus hinting at the non-reliability

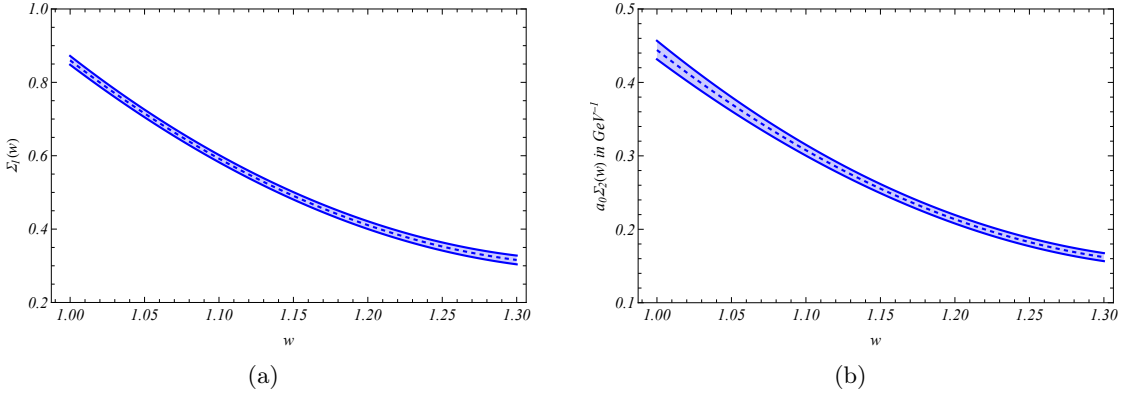


Figure 4: Plots showing the w distribution of $\Sigma_1(w)$ and $a_0\Sigma_2(w)$.

of the approach at the low q^2 region. Hence we restrict the validity of the above results upto $w = 1.3$.

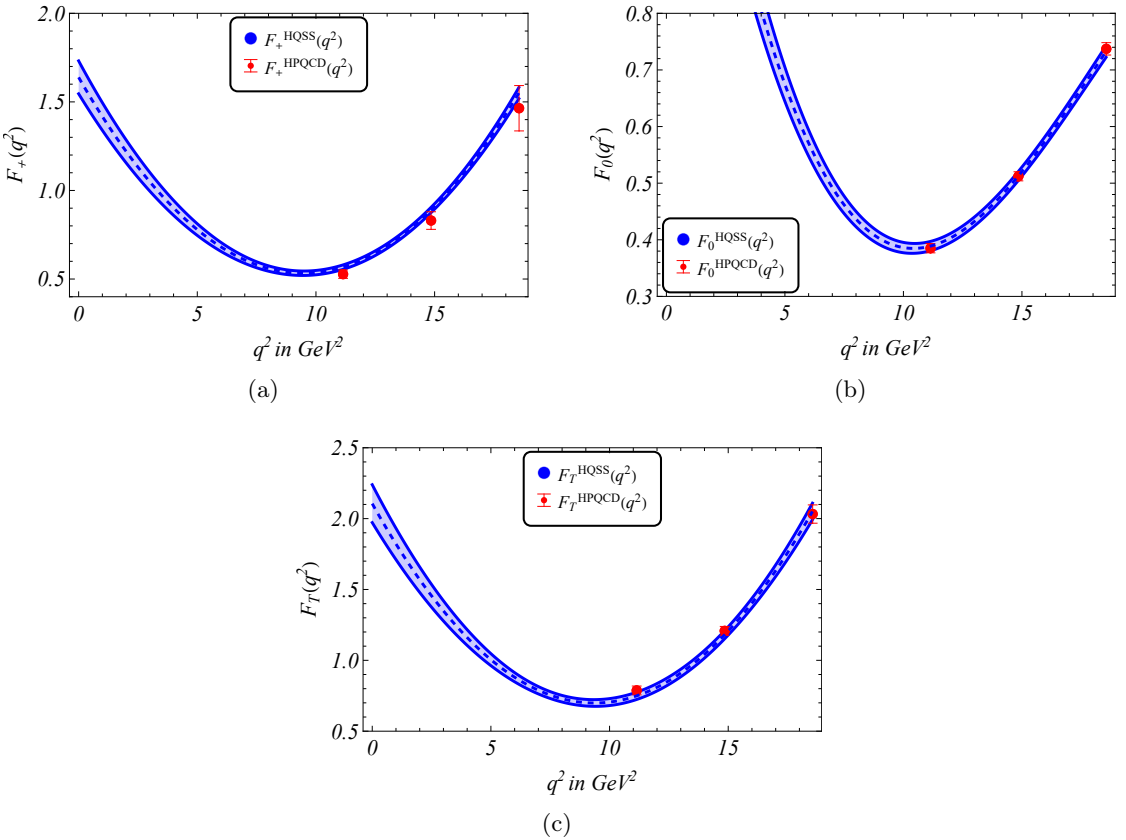


Figure 5: Plots showing the q^2 distribution of $B_c \rightarrow D_s$ form factors F_+ , F_0 and F_T . The red markers denote the synthetic data points generated using the BCL parameters supplied by HPQCD.

4.3 Obtaining q^2 distribution of rest of the $B_c \rightarrow D_s^*$ form factors

Once we have information on the soft functions near $w = 1$, we can use them in eqns.(4.13) and (4.14) to obtain information of all the $B_c \rightarrow D_s^*$ form factors at high q^2 region. But as we just saw, this approach does not give reliable results for low and mid q^2 region. To obtain the shape in this region, we adopt a suitable parametrization method. In this work, we employ the BGL parametrization due to its model-independent foundation. The parametrization is done by mapping the physical q^2 region onto a disk $|z| \leq 1$ via conformal transformation $q^2 \rightarrow z$, where z is the new kinematic variable. Each form factor can then be expressed as a convergent power series in the variable z , ensuring a well-behaved expansion. This parametrization method also respects analyticity and crossing symmetry, and eliminates unphysical singularities associated with intermediate resonances through an appropriate pole factor. The form factors in this parametrization, defined through a z -expansion, take the form

$$f_i(q^2) = \frac{1}{P_i(q^2)\phi_i(q^2)} \sum_{n=0}^N a_n^i z(q^2)^n, \quad (4.16)$$

where a_n^i are the expansion coefficients that encode the shape of each of the form factors over the kinematic region. These coefficients are intrinsically constrained by the unitarity condition

$$\sum_{n=0}^N |a_n^i|^2 \leq 1. \quad (4.17)$$

The conformal variable $z(q^2, t_0)$ is defined as

$$z(q^2, t_0) = \frac{\sqrt{t_+ - q^2} - \sqrt{t_+ - t_0}}{\sqrt{t_+ - q^2} + \sqrt{t_+ - t_0}}, \quad (4.18)$$

with $t_+ = (m_{B_0} + m_{K/K^*})^2$ and t_0 , an arbitrary reference point is chosen to be [51]

$$t_0 = t_{opt} = t_+ \left(1 - \sqrt{1 - \frac{t_-}{t_+}} \right), \quad (4.19)$$

to center the z -expansion around mid q^2 region, so as to facilitate a faster convergence¹.

At this point, an issue needs to be addressed with the current form-factor convention. The issue mainly arises during the calculation of $\phi_i(q^2)$, the outer function, whose form is chosen to be such that the unitarity constraints are satisfied. Checking the formalism described in section 3.3 of [52], the authors write the unitarity inequality as

$$\frac{1}{\pi} \int_{t_+}^{\infty} \frac{dt}{t - t_0} \sqrt{\frac{t_+ - t_0}{t - t_+}} |\phi_i(t) A_i(t)|^2 \leq 1, \quad (4.20)$$

¹Note that in this work we adopt a different choice of t_0 compared to HPQCD [39]. This choice of t_0 maps the physical semileptonic region into a symmetric interval in z , i.e., $z(q^2 = 0) = z(q^2 = t_-)$, so that the physical q^2 region corresponds to $-z_{max} \leq z \leq z_{max}$. As a result, the maximum $|z|$ is minimized, which means the truncated z -series converges much faster compared to either $t_0 = 0$ or $t_0 = t_-$.

where $A_i(q^2)$ represent the helicity-based form factors, and i runs over each helicity basis. Now these form factors have been calculated to be [52]

$$|A_T^{V-A}|^2 = \sum_{i=0}^2 |\mathcal{B}_{V,i}|^2, \quad |A_L^{V-A}|^2 = 3|\mathcal{B}_{V,t}|^2, \quad |A_T^{T+AT}|^2 = q^2 \sum_{i=0}^2 |\mathcal{B}_{T,i}|^2, \quad (4.21)$$

where for vector and axial-vector currents, the form factors are given by [52]

$$\begin{aligned} \mathcal{B}_{V,0}(q^2) &= \frac{(M+m)(M^2-m^2-q^2)A_1(q^2)-\lambda(q^2)A_2(q^2)}{2m\sqrt{\lambda(q^2)}(M+m)}, \\ \mathcal{B}_{V,1}(q^2) &= \frac{\sqrt{2q^2}}{M+m}V(q^2), \\ \mathcal{B}_{V,2}(q^2) &= \frac{\sqrt{2q^2}(M+m)}{\sqrt{\lambda(q^2)}}A_1(q^2), \\ \mathcal{B}_{V,t}(q^2) &= A_0(q^2), \end{aligned} \quad (4.22)$$

and for tensor currents, the form factors are given by

$$\begin{aligned} \mathcal{B}_{T,0}(q^2) &= \sqrt{q^2} \frac{(M^2-m^2)(M^2+3m^2-q^2)T_2(q^2)-\lambda(q^2)T_3(q^2)}{2m\sqrt{\lambda(q^2)}(M^2-m^2)}, \\ \mathcal{B}_{T,1}(q^2) &= \sqrt{2}T_1(q^2), \\ \mathcal{B}_{T,2}(q^2) &= \frac{\sqrt{2}(M^2-m^2)}{\sqrt{\lambda(q^2)}}T_2(q^2). \end{aligned} \quad (4.23)$$

Now, if we continue our analysis in the current form factor convention, $|A_T^{V-A}|^2$ would give terms like $\text{Re}(A_1^*A_2)$ and $\text{Re}(A_1A_2^*)$ along with the usual $|A_1|^2$ and $|A_2|^2$ terms. Similarly $|A_T^{T+AT}|^2$ would give terms like $\text{Re}(T_2^*T_3)$ and $\text{Re}(T_2T_3^*)$ along with the usual $|T_2|^2$ and $|T_3|^2$ terms. These cross terms lead to a non-diagonal structure in the unitarity relations. Because of this mixing, it would become impossible to define unique outer functions $\phi_i(q^2)$ for each form factor individually, as the unitarity bound no longer factorizes into independent form factors. To resolve this issue the authors in [52, 53] suggested shifting the form factors to the helicity basis, where the form factors A_2 and T_3 get replaced by A_{12} and T_{23} , defined as

$$\begin{aligned} A_{12} &= \frac{(M+m)^2(M^2-m^2-q^2)A_1-\lambda(q^2)A_2}{16Mm^2(M+m)}, \\ T_{23} &= \frac{(M^2-m^2)(M^2+3m^2-q^2)T_2-\lambda(q^2)T_3}{8Mm^2(M-m)}. \end{aligned} \quad (4.24)$$

This choice of form factor basis eliminates all the cross terms and thus diagonalizes the unitarity relations. Also, we can now separately extract the outer functions for each form factor. Henceforth, we will be performing all our calculations using helicity basis form factors. The form of the outer function has been obtained by [53] as

$$\phi_i(q^2) = \sqrt{\frac{\mathcal{N}_F \eta^{b \rightarrow s}}{32\pi^2 \chi_i}} \left(\frac{\lambda(q^2)}{-z(q^2, t_-)} \right)^{\frac{m}{4}} \left(\frac{-z(q^2, 0)}{q^2} \right)^{\frac{n+p+1}{2}} \sqrt{\frac{4(1+z(q^2, t_0))(t_+ - t_0)}{(z(q^2, t_0) - 1)^3}}. \quad (4.25)$$

Construction of the outer function $\phi_i(q^2)$ originates from the short-distance two-point correlator of the quark current and is therefore independent of the spectator quark. Consequently, we can use the same functional form and the relevant parameters universally for all transitions mediated by the same quark current. This allows us to adopt the same analytical form of $\phi_i(q^2)$ and the corresponding χ_i functions derived for $b \rightarrow s$ transitions in [52, 53], while replacing relevant kinematic quantities. The parameters \mathcal{N}_F, p, n, m are form factor specific and are listed in table 8.

Form factor	\mathcal{N}_F	p	n	m
A_0	1	2	1	3
A_1	$2t_+$	1	2	1
A_{12}	$64M^2m^2$	2	2	1
V	$2/t_+$	1	2	3
T_1	2	1	3	3
T_2	$2t_+t_-$	1	3	1
T_{23}	$16M^2m^2/t_+$	0	3	1

Table 8: Parameters of the outer function for $B_c \rightarrow D_s^*$ form factors.

Additionally, the outer function depends on χ_i coefficient, which is a perturbatively calculable short-distance coefficient that comes from the derivative of two point current-current correlator:

$$\chi_i = \frac{1}{2} \frac{d^n}{dq^{2n}} \Pi_i(q^2) \Big|_{q^2=0}, \quad (4.26)$$

where $\Pi_i(q^2)$ is the two-function correlation function. The values of χ_i used in this work are shown in table 9, and have been taken from [52]

Form Factor	A_0	A_1	A_{12}	V	T_1	T_2	T_{23}
$\chi_i \times 10^2$	1.57	$1.13/m_b^2$	$1.13/m_b^2$	$1.20/m_b^2$	$0.803/m_b^2$	$0.748/m_b^2$	$0.748/m_b^2$

Table 9: List of the functions χ_i for each form factor considered in this work.

Finally, the function $P_i(q^2)$ represents the Blaschke factor and prevents divergence in the BGL expansion by factoring out known resonance poles from the form factors, thus ensuring that the remaining piece is analytic and can be safely expanded in a rapidly converging power series in $z(q^2, t_0)$. It has the form

$$P_i(q^2) = \prod_{res} \frac{z(q^2, t_0) - z(M_{i,res}^2, t_0)}{1 - z(q^2, t_0)z(M_{i,res}^2, t_0)}, \quad (4.27)$$

where the product runs over each resonance state. $M_{i,res}$ represents the B_s^* resonance masses, values of which used in this work are shown in table 10, and has been taken from

Form Factor	A_0	A_1	A_{12}	V	T_1	T_2	T_{23}
$M_{i,res}$ in GeV	5.366	5.829	5.829	5.415	5.415	5.829	5.829

Table 10: Masses of the low lying B_s^* resonances.

[54]. Since we are only considering the lowest-lying resonance state for each form factor, the Blaschke factor reduces to a single pole form.

With the z -expansion expressions of the form factors and the corresponding form factor inputs obtained using eqns.(4.13) and (4.14) and presented in tables 21 and 22, we can construct a chi-square function with the BGL coefficients as free parameters. But these inputs would constrain the form factor shape only at high q^2 region. To constrain the shapes at low q^2 region, we take pQCD form factor values at $q^2 = 0$, previously presented in table 6, as additional inputs into the chi-square function². Once the total chi-square function is constructed, we then minimize it to extract the required BGL coefficients, estimates of which are given in table 11 along with the corresponding correlation matrix in table 25.

Form factors	a_0	a_1	a_2
A_0	0.0844(15)	-0.396(29)	0.788(354)
A_1	0.0349(8)	-0.116(16)	0.723(172)
A_{12}	-	-0.029(6)	0.295(66)
V	0.0950(30)	-0.340(48)	0.286(258)
T_1	0.0460(8)	-0.183(13)	0.436(156)
T_2	-	-0.058(5)	0.167(59)
T_{23}	0.0369(20)	-0.417(44)	0.851(401)
DOF	7		
χ^2_{min}/DOF	2.272		
p-Value	2.62%		

Table 11: Extracted BGL coefficients for $B_c \rightarrow D_s^*$ form factors.

A point to be noted from table 11 is that we have not included the coefficients a_0 for A_2 and T_2 . This omission is done to respect the QCD constraints, previously discussed in eqn.(2.27), and satisfied by the form factors at $q^2 = 0$, making a_0 for A_2 a function of BGL coefficients of A_0 and A_1 , and a_0 for T_2 a function of BGL coefficients of T_1 . Hence, treating

²It is to be noted that the form factors calculated using pQCD and universal functions were in the previous basis, $A_{0,1,2}$, V and $T_{1,2,3}$. Before incorporating these inputs into the chi-square function, we have transformed them into the helicity basis by computing the corresponding A_{12} and T_{23} form factors using eqn.(4.24)

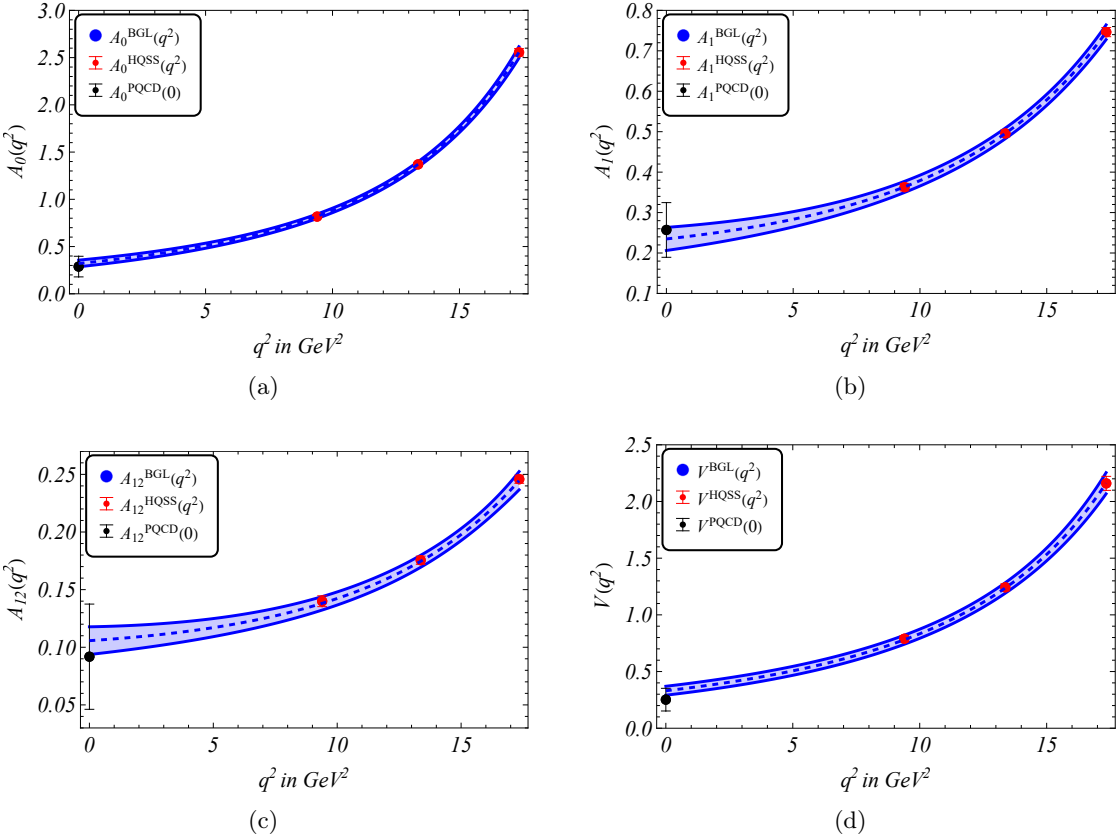


Figure 6: q^2 distribution of $B_c \rightarrow D_s^*$ vector and axial-vector form factors. The blue curve denotes the distribution obtained using the extracted BGL coefficients, the red and black markers denote the form factor values obtained using the extracted soft functions and pQCD, respectively.

a_0 for A_2 and T_2 as free parameters would violate these known QCD relations and induce redundancy during the chi-square minimization.

We also observe that the chi-square minimization yields a very poor goodness of fit estimate, i.e., $\chi^2_{\min}/\text{DOF} > 1$. This is primarily due to the very precise error estimates of the form factor inputs, ranging between 1.5-6.5%, and the coefficients being constrained by unitarity constraints. To account for this, Birge's rescaling is adopted, a method of rescaling the error estimate adopted by FLAG in [55]. The error estimates of the extracted coefficients are rescaled by a factor of $\chi^2_{\min}/\text{DOF} = \sqrt{15.901/7} = 1.507$. The correlation matrix, however, remains unaffected by this rescaling.

Furthermore, we observe that error estimates of the parameters for each form factor increases as we go up in order of z-expansion series, thus signifying a reducing sensitivity of the form factor slopes with increasing order of the parameters. Further we also observe that the extracted parameters follow the hierarchy $a_2 z(q^2)^2 < a_1 z(q^2) < a_0$, implying that our z-expansion is converging in nature. Additionally, since we have truncated the BGL series up to quadratic order, i.e., up to z^2 , we introduce an additional error to take into

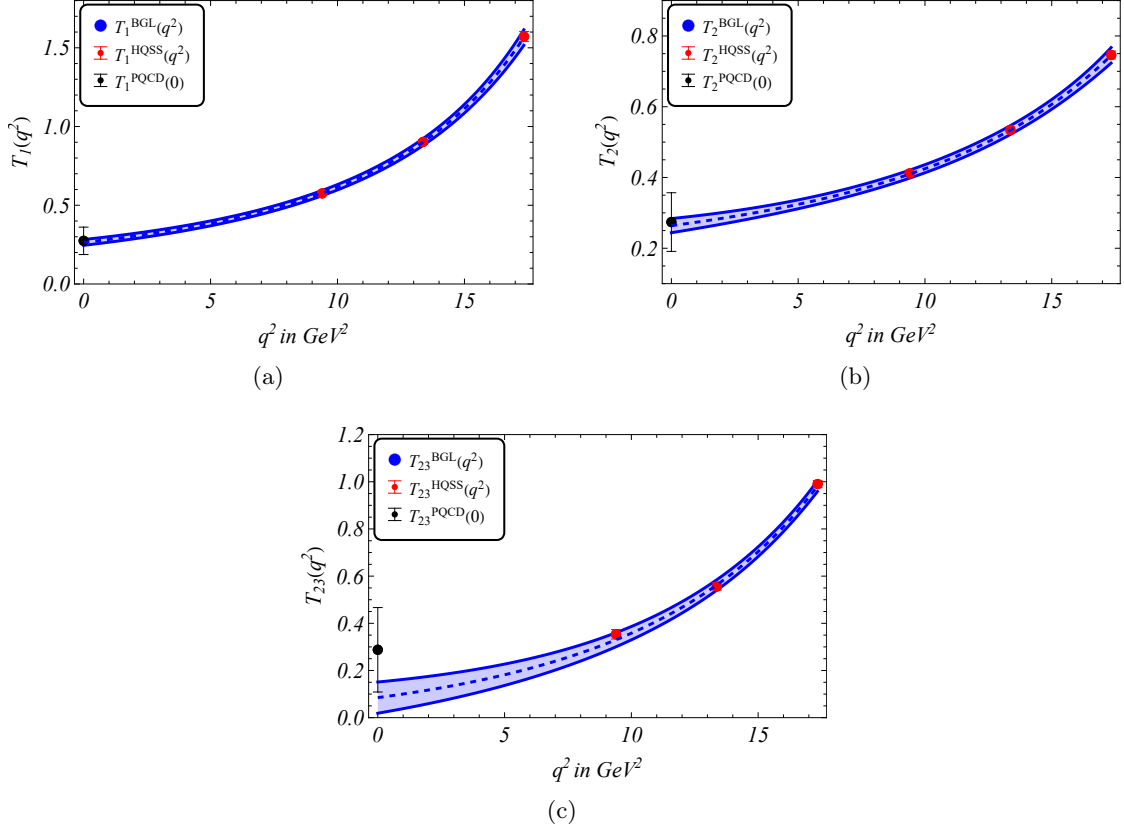


Figure 7: q^2 distribution of $B_c \rightarrow D_s^*$ tensor form factors. The blue curve denotes the distribution obtained using the extracted BGL coefficients, the red and black markers denote the form factor values obtained using the extracted soft functions and pQCD, respectively.

account the error associated with missing higher-order terms. In particular, we estimate the possible effect of the next higher-order term in the expansion, i.e., z^3 , neglecting the relatively small higher-order terms after that, as prescribed in [40]. We then propagate this additional error as a systematic uncertainty into the form factors. The estimate of this systematic error is defined as follows:

$$\delta f_i(q^2) = \frac{a_3^{\max} |z(q^2)^3|}{P(q^2)}, \quad (4.28)$$

where a_3^{\max} represents the maximum possible value of $|a_3|$ for each individual form factor and is estimated by using the unitarity constraints, where the coefficients $a_{0,1,2}$ are already extracted in table 11. With all the BGL coefficients extracted and truncation uncertainty included, we have all the information necessary to get the q^2 distribution of the form factors over the full semileptonic region. In figures 6 and 7 we showcase these q^2 distribution plots.

5 Prediction of physical observables

With the $B_c \rightarrow D_s^*$ form factors defined and their information over the full physical q^2 region available to us, we are now in a position to predict some of the important physical observables. In subsection 5.1 we present our prediction of branching fractions of some of the relevant decay channels. In subsection 5.2 we perform a full angular analysis of FCNC process and present predictions of relevant observables.

5.1 Decay Width and branching fractions

For the $B_c^- \rightarrow D_s^{*-} \ell^+ \ell^-$ and $B_c^- \rightarrow D_s^{*-} \nu \bar{\nu}$ FCNC processes governed by $b \rightarrow s$ quark-level transition, the differential decay width is taken from subsection 2.1.1. It is then integrated over the full physical q^2 region, i.e., $q^2 \in (4m_\ell^2, (M - m)^2)$, and multiplied by τ_{B_c} to obtain the branching fractions of the respective mode. We present our predictions for these branching fractions, along with a comparison with previous pQCD predictions, in table 12. These channels are more interesting since these are mediated exclusively by neutral current processes, and hence have a highly suppressed branching ratio, making them highly sensitive to possible physics beyond the SM.

Decay Modes	This work	Previous PQCD[26]
$\mathcal{B}(B_c^- \rightarrow D_s^{*-} \ell^+ \ell^-)$	$4.741(302) \times 10^{-7}$	$4.40^{+2.11}_{-1.76} \times 10^{-7}$
$\mathcal{B}(B_c^+ \rightarrow D_s^{*+} \ell^+ \ell^-)$	$4.735(300) \times 10^{-7}$	-
$\mathcal{B}(B_c^- \rightarrow D_s^{*-} \tau^+ \tau^-)$	$0.469(49) \times 10^{-7}$	$0.52^{+0.26}_{-0.22} \times 10^{-7}$
$\mathcal{B}(B_c^+ \rightarrow D_s^{*+} \tau^+ \tau^-)$	$0.468(50) \times 10^{-7}$	-
$\mathcal{B}(B_c^- \rightarrow D_s^{*-} \nu \bar{\nu})$	$3.541(119) \times 10^{-6}$	$4.04^{+1.96}_{-1.62} \times 10^{-6}$

Table 12: Predictions for the branching fractions of the $B_c \rightarrow D_s^*$ FCNC transitions with ($l = e, \mu$) along-with comparison with predictions in existing literature.

In the results of table 12, the primary contribution to the total uncertainty originates from the form factors, resulting in an overall uncertainty of about 4-9% for the three channels considered. Our results exhibit a significant improvement in percentage error when compared to previous pQCD predictions. Additionally, we can define an LFUV observable by taking the ratio of branching fractions of the τ and ℓ modes. The observable is defined as

$$R^{B_c^- \rightarrow D_s^{*-}} = \frac{\mathcal{B}(B_c^- \rightarrow D_s^{*-} \tau^+ \tau^-)}{\mathcal{B}(B_c^- \rightarrow D_s^{*-} \ell^+ \ell^-)} = 0.0988(40), \quad (5.1)$$

where as expected, we observe the error percentage to be quite small. This can be tested once experimental measurements start to come up in future.

Furthermore, we also observe a difference in the predictions of $\mathcal{B}(B_c^- \rightarrow D_s^{*-} \ell^+ \ell^-)$ channels and their respective CP-conjugate modes. This difference hints towards a non-zero value of CP asymmetry, thus making prediction of the CP asymmetry observable

significant. The observable is defined as

$$\mathcal{A}_{CP}(q^2) = \frac{d\mathcal{B}(B_c^- \rightarrow D_s^{*-} \ell^+ \ell^-)/dq^2 - d\mathcal{B}(B_c^+ \rightarrow D_s^{*+} \ell^+ \ell^-)/dq^2}{d\mathcal{B}(B_c^- \rightarrow D_s^{*-} \ell^+ \ell^-)/dq^2 + d\mathcal{B}(B_c^+ \rightarrow D_s^{*+} \ell^+ \ell^-)/dq^2}, \quad (5.2)$$

and the q^2 averaged values of this observable, integrated over the full physical q^2 region, are presented in table 13.

Decay Mode	Our prediction
$\langle \mathcal{A}_{CP} \rangle (B_c \rightarrow D_s^* \ell^+ \ell^-)$	$6.567(151) \times 10^{-4}$
$\langle \mathcal{A}_{CP} \rangle (B_c \rightarrow D_s^* \tau^+ \tau^-)$	$3.921(37) \times 10^{-4}$

Table 13: Predictions for CP asymmetry of the respective decay channels.

From table 13 we can see that the CP asymmetry, although small, but remains non-zero. This non-vanishing value stems primarily from the phase terms carried by the CKM elements V_{ub} within the effective coefficient C_9^{eff} . A comparison of the second row highlights the suppression in the τ -lepton case arising due to heavy lepton mass effects and reduced phase space.

5.2 Angular Observables

Following the prediction on branching fractions in the previous subsection, we next shift our focus onto studying the cascade decay mode $B_c^- \rightarrow D_s^{*-} (\rightarrow D_s^- \pi^0) \ell^+ \ell^-$, and present predictions on a number of angular observables and some other observables derived from them, as was briefed in section 2.1.2.

We start by presenting our results on the CP average angular coefficients S_i . In figure 8 we present the q^2 distribution of each of these angular coefficients. The blue and red curves denote the distribution of observables corresponding to the light and heavy lepton modes respectively, and the grey bands denote the regions of J/ψ and $\psi(2S)$ resonances. From figure 8 we can see that the observables S_4 , S_5 , S_{6s} , S_8 and S_9 have a zero crossing within the physical q^2 region. However, S_4 , S_8 and S_9 are themselves not clean and have very high sensitivity to hadronic inputs like form factors, making them highly sensitive to the choice of form factor parametrization and hence their zero crossing point is not that reliable. For S_8 and S_9 , this point becomes relevant if we study possible NP scenarios. Therefore, we quote zero crossing q^2 points for the S_5 and S_{6s} , which are

$$S_5 : q_0^2 = 1.89(16) \text{ GeV}^2, \quad S_{6s} : q_0^2 = 3.26(24) \text{ GeV}^2. \quad (5.3)$$

These points are interesting because they indicate a complete cancellation of the effects of left- and right-handed transversity amplitudes. Any higher-order QCD or non-factorizable corrections that modify these amplitudes will shift the zero point from the obtained values, thereby giving us an idea of the impact of corrections on these observables. Also, these points are sensitive to any possible new physics effects, since a small change in the Wilson coefficients will drastically change the zero crossing points. Out of all the observables,

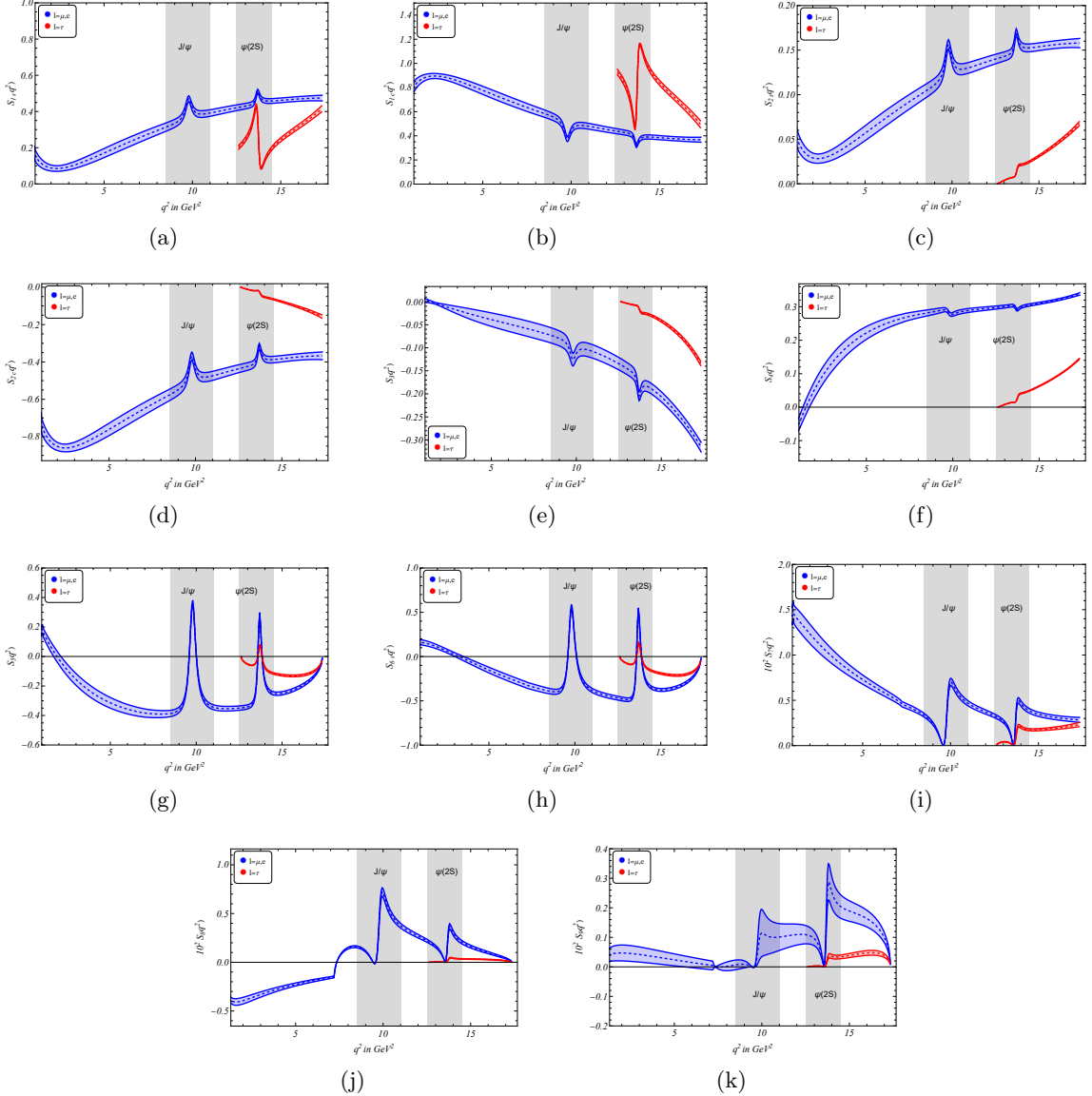


Figure 8: The q^2 dependence of normalized CP averaged angular observables S_i . The blue and the red plots depict our results for the light lepton and τ lepton modes respectively and the gray bands denote the region of J/ψ and $\psi(2S)$ resonances.

the zero crossing point of S_{6s} is the most important one, since this directly gives the q^2 point where the forward-backward asymmetry also becomes zero, a point where the forward and backward rates of the decay process exactly balance each other. We also calculate q^2 averaged values of these observables separated into four q^2 bins and present the evaluated values in table 14.

The q^2 limits in each bin are chosen as follows:

- For the first q^2 bin, the lower limit should ideally be $4m_l^2$. But in our analysis we have set it at $q^2 = 1.1 \text{ GeV}^2$. This is because at small q^2 value, the relevant decay amplitude

q^2 bins (GeV^2)	$\langle S_{1s} \rangle$		$\langle S_{1c} \rangle$		$\langle S_{2s} \rangle$		$\langle S_{2c} \rangle$	
Lepton Mode:	$l = \mu, e$	$l = \tau$	$l = \mu, e$	$l = \tau$	$l = \mu, e$	$l = \tau$	$l = \mu, e$	$l = \tau$
[1.1, 6.0]	0.135(14)	-	0.827(19)	-	0.045(5)	-	-0.800(18)	-
[6.0, 8.0]	0.259(26)	-	0.657(35)	-	0.086(9)	-	-0.647(35)	-
[11.0, 12.5]	0.407(17)	-	0.458(23)	-	0.135(6)	-	-0.454(23)	-
[15.0, 17.0]	0.468(14)	0.312(13)	0.376(18)	0.458(22)	0.156(4)	0.044(1)	-0.375(18)	-0.107(5)
q^2 bins (GeV^2)	$\langle S_3 \rangle$		$\langle S_4 \rangle$		$\langle S_5 \rangle$		$\langle S_{6s} \rangle$	
Lepton Mode:	$l = \mu, e$	$l = \tau$	$l = \mu, e$	$l = \tau$	$l = \mu, e$	$l = \tau$	$l = \mu, e$	$l = \tau$
[1.1, 6.0]	-0.025(6)	-	0.148(15)	-	-0.185(26)	-	-0.063(17)	-
[6.0, 8.0]	-0.058(17)	-	0.264(13)	-	-0.380(27)	-	-0.309(35)	-
[11.0, 12.5]	-0.121(15)	-	0.293(5)	-	-0.352(17)	-	-0.434(23)	-
[15.0, 17.0]	-0.243(10)	-0.071(3)	0.320(3)	0.091(1)	-0.206(10)	-0.125(6)	-0.332(15)	-0.202(10)
q^2 bins (GeV^2)	$10^2 \times \langle S_7 \rangle$		$10^2 \times \langle S_8 \rangle$		$10^2 \times \langle S_9 \rangle$			
Lepton Mode:	$l = \mu, e$	$l = \tau$	$l = \mu, e$	$l = \tau$	$l = \mu, e$	$l = \tau$		
[1.1, 6.0]	0.945(44)	-	-0.293(13)	-	0.034(14)	-		
[6.0, 8.0]	0.485(31)	-	-0.062(4)	-	0.005(6)	-		
[11.0, 12.5]	0.389(23)	-	0.289(19)	-	0.107(40)	-		
[15.0, 17.0]	0.313(24)	0.193(16)	0.102(11)	0.027(3)	0.162(27)	0.045(7)		

Table 14: q^2 averaged estimates of the various CP averaged angular observables S_i in separate q^2 bins.

is dominated mostly by the photon pole, and hence by just one Wilson Coefficient C_7^{eff} . Considering this region into the analysis will not add any new information in comparison to what is already available from analysis of $b \rightarrow s\gamma$ channel. Additionally including the small q^2 region might introduce contributions due to light resonances like ρ , ω and ϕ [21]. Hence we avoid this region. The upper limit of $q^2 = 6.0 GeV^2$ is taken to avoid the J/ψ resonance peak at $m_{J/\psi}^2 = 9.6 GeV^2$ by a safe margin, and also to stay in accordance to experimental conventions.

- For the second q^2 bin, we continue from the first bin, setting the lower limit at $q^2 = 6.0 GeV^2$. As for the upper limit, we set $q^2 = 8.0 GeV^2$ to stay below the J/ψ resonance. A point to note is that, instead of having a single bin in the range $q^2 \in (1.1, 8.0) GeV^2$, we have divided the q^2 range into two bins. This is because the range $6.0 - 8.0 GeV^2$ lies close to the J/ψ resonance and the non-local $c\bar{c}$ resonance effects are non-negligible in this region, while the range $1.1 - 6.0 GeV^2$ does not suffer from any such contributions. Hence mixing the two regions will contaminate the clean predictions in the low q^2 region.
- For the third q^2 bin, the q^2 range is chosen to lie in the region between the J/ψ and $\psi(2S)$ resonances. For the lower limit, we set it at $q^2 = 11.0 GeV^2$, a value conveniently above J/ψ resonance, while for the upper limit we set it at $q^2 = 12.5 GeV^2$, safely below the $\psi(2S)$ resonance peak.

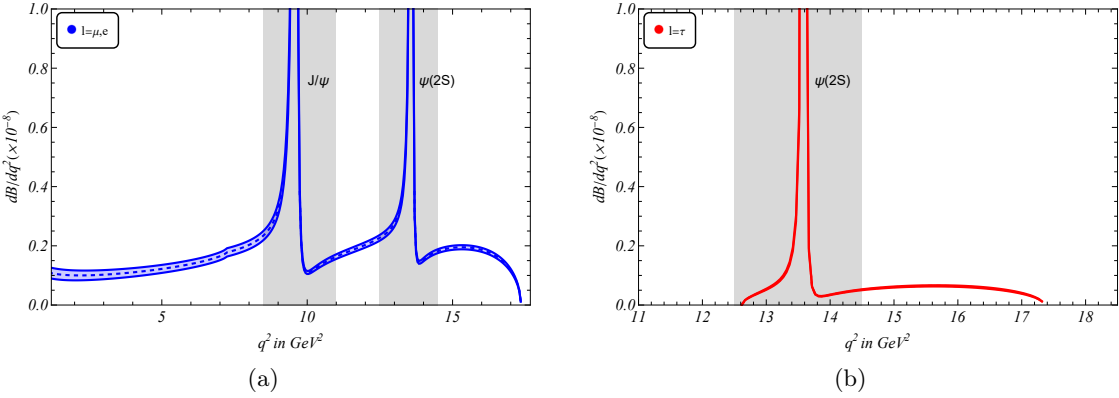


Figure 9: The q^2 dependence of differential branching fractions $d\mathcal{B}/dq^2$ of $B_c^- \rightarrow D_s^{*-}(\rightarrow D_s^- \pi^0) \ell^+ \ell^-$. The first plot depicts our result for the light lepton mode, and the second plot depicts our result for the τ lepton mode, and the gray bands denote the region of J/ψ and $\psi(2S)$ resonances.

- For the fourth q^2 bin, we choose the lower limit at $q^2 = 15.0 \text{ GeV}^2$, a value greater than the $\psi(2S)$ resonance peak. The upper limit of $q^2 = 17.0 \text{ GeV}^2$ is chosen to be in accordance with experimental convention.

From figure 8 and table 14, we can see that among the observables S_{1s} to S_5 , S_3 has a smaller magnitude compared to the other observables, but is comparable to S_{6s} . This is primarily due to partial cancellation between the transversity amplitudes, as can be seen in eqn.(2.8). The cancellation becomes weaker as we move from the first to the fourth bin, leading to an increase in the absolute value. The reason for this can be traced back to analytic expressions in eqn.(A.1), where it can be clearly seen that they are dependent upon the imaginary part of the transversity amplitudes, and hence of the Wilson Coefficients C_7^{eff} and C_9^{eff} , whose imaginary parts, upon checking numerically, is found out to be highly suppressed compared to the real part.

Next, we calculate the CP-averaged branching fraction, taking the expressions previously discussed in eqn.(2.13) and multiplying them by τ_{B_c} . In figure 9 we present q^2 distribution of branching fractions for the light and heavy lepton modes. Following this, in table 15 we calculate q^2 averaged values of the branching fractions in the same four q^2 bins, i.e., $[1.1, 6.0]$, $[6.0, 8.0]$, $[11.0, 12.5]$ and $[15.0, 17.0] \text{ GeV}^2$.

We have verified the results of table 15 by calculating $\mathcal{B}(B_c^- \rightarrow D_s^{*-}(\rightarrow D_s^- \pi^0) \ell^+ \ell^-)$ from expressions of $\mathcal{B}(B_c^- \rightarrow D_s^{*-} \ell^+ \ell^-)$ in terms of Helicity amplitudes and discussed in section 2.1.1, and then multiplying it by $\mathcal{B}(D_s^{*-} \rightarrow D_s^- \pi^0)$, in each q^2 bin. Additionally, we also check for lepton flavor universality by calculating the ratio between heavy and light lepton branching fractions in the fourth q^2 bin, defined as

$$R^{\tau\mu} = \frac{\mathcal{B}(B_c^- \rightarrow D_s^{*-}(\rightarrow D_s^- \pi^0) \tau^+ \tau^-)}{\mathcal{B}(B_c^- \rightarrow D_s^{*-}(\rightarrow D_s^- \pi^0) \ell^+ \ell^-)}, \quad (5.4)$$

and is found to be 0.335(4) in this work.

q^2 bins (GeV^2)	$\mathcal{B}(l = e, \mu)$	$\mathcal{B}(l = \tau)$
[1.1, 6.0]	0.549(46)	-
[6.0, 8.0]	0.337(27)	-
[11.0, 12.5]	0.290(13)	-
[15.0, 17.0]	0.354(13)	0.118(4)

Table 15: q^2 averaged estimates of branching fractions ($\times 10^{-8}$) of $B_c^- \rightarrow D_s^{*-} (\rightarrow D_s^- \pi^0) \ell^+ \ell^-$ in separate q^2 bins.

After the CP averaged observables and branching fractions, we next focus on some of the more established observables. These are the forward backward asymmetry A_{FB} , and the D_s^* longitudinal and transverse polarization fractions F_L and F_T respectively. We take the expressions previously discussed in eqns.(2.14) and (2.15) in subsection 2.1.2. We present q^2 distribution of these observables in figure 10.

We also compute the q^2 averaged values of these observables by calculating

$$\langle \mathcal{A} \rangle = \frac{\int_{q_{min}^2}^{q_{max}^2} \mathcal{A}(q^2) \left(\frac{d\Gamma}{dq^2} + \frac{d\bar{\Gamma}}{dq^2} \right) dq^2}{\int_{q_{min}^2}^{q_{max}^2} \left(\frac{d\Gamma}{dq^2} + \frac{d\bar{\Gamma}}{dq^2} \right) dq^2}, \quad (5.5)$$

where $\mathcal{A} = A_{FB}$, F_L or F_T . We perform our calculations in four separate q^2 bins, and present them in table 16.

q^2 bins (GeV^2)	$\langle A_{FB} \rangle$		$\langle F_L \rangle$		$\langle F_T \rangle$	
Lepton Mode:	$l = \mu, e$	$l = \tau$	$l = \mu, e$	$l = \tau$	$l = \mu, e$	$l = \tau$
[1.1, 6.0]	-0.049(19)	-	0.817(29)	-	0.183(29)	-
[6.0, 8.0]	-0.232(26)	-	0.655(35)	-	0.345(35)	-
[11.0, 12.5]	-0.326(17)	-	0.457(23)	-	0.543(23)	-
[15.0, 17.0]	-0.249(12)	-0.152(7)	0.376(18)	0.406(92)	0.624(18)	0.446(18)

Table 16: q^2 averaged estimates of forward backward asymmetry, longitudinal and transverse polarization fractions in separate q^2 bins.

Further, we also present predictions for the clean angular observables $P_{1,2,3}$ and $P'_{4,5,6,8}$, as defined in eqn.(2.16). These observables are of particular interest due to their reduced sensitivity to the hadronic form factors, rendering them comparatively cleaner and less affected by hadronic uncertainties. As a result, they serve as powerful probes for exploring potential new physics (NP) effects. The q^2 distribution of these observables is presented in figure 11.

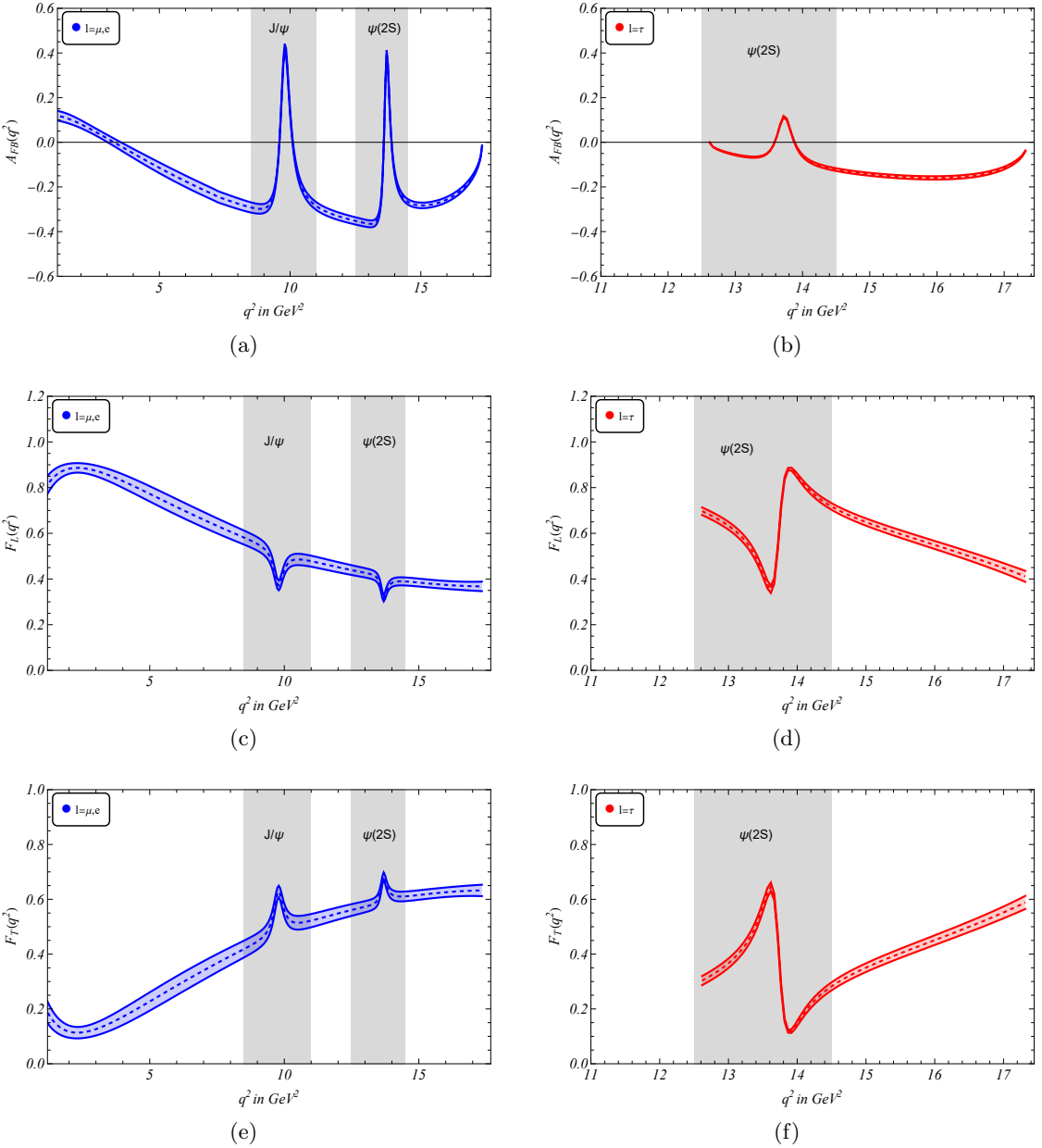


Figure 10: The q^2 dependence of lepton forward-backward asymmetry parameter A_{FB} , D_s^* longitudinal and transverse polarization fractions F_L and F_T in $B_c \rightarrow D_s^* \rightarrow D_s^- \pi^0 l^+ l^-$ channel. The blue plots denote the results for light lepton modes and the red plots denote the results for tau lepton mode and the gray bands denote the region of J/ψ and $\psi(2S)$ resonances.

Additionally, we also present predictions for the average values of these observables in the four q^2 bins in table 17. We have verified two of the observables, particularly P_2 and

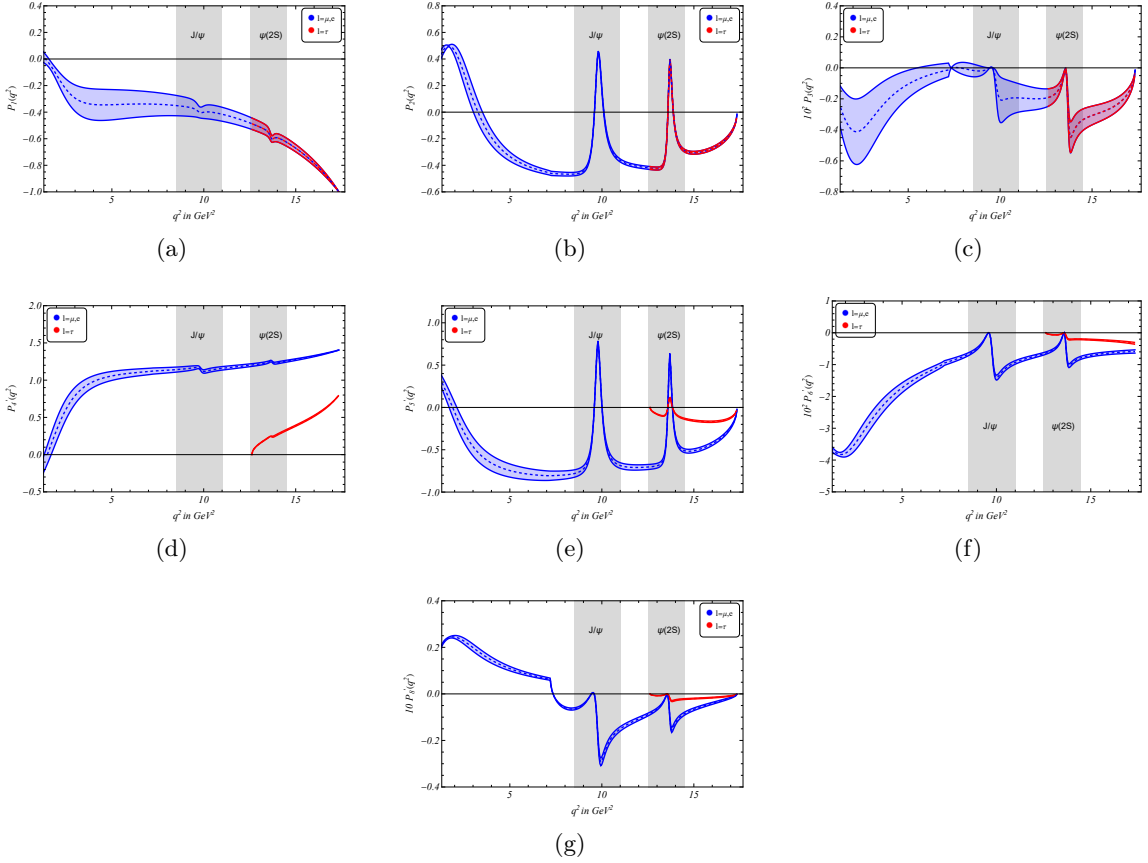


Figure 11: The q^2 dependence of clean angular observables $P_{1,2,3}$ and $P'_{4,5,6,8}$. The blue and the red plots depict our results for the light lepton and τ lepton modes respectively and the gray bands denote the region of J/ψ and $\psi(2S)$ resonances.

P'_5 using the relations [56]

$$P_2 = \frac{2}{3} \cdot \frac{A_{FB}}{1 - F_L}, \quad P'_5 = \frac{S_5}{\sqrt{F_L(1 - F_L)}}, \quad (5.6)$$

and have found the results in the table to be in good agreement with each other. Further, from table 17 we observe that P_3 exhibits the smallest magnitude across all four q^2 bins. This behaviour is expected, since P_3 is proportional to the angular observable S_9 , which is defined through the imaginary part of the interference term ($\mathcal{A} \parallel L^* \mathcal{A} \perp L - L \leftrightarrow R$). In the Standard Model, this term is strongly suppressed due to the small relative strong phases between the transversity amplitudes, resulting in a negligibly small value of S_9 , and consequently of P_3 .

In table 17, it is worth noting that the observables P_1 , P_2 and P_3 exhibit about 2-3% difference between light and heavy lepton modes. This suggests that the transversity amplitudes governing these observables are largely insensitive to lepton mass effects in the high q^2 region. In contrast, the primed observables P'_4 , P'_5 , P'_6 and P'_8 exhibit significant deviation between light and heavy lepton modes. Furthermore, we also observe that the

q^2 bins (GeV^2)	$\langle P_1 \rangle$		$\langle P_2 \rangle$		$10^2 \times \langle P_3 \rangle$			
Lepton Mode:	$l = \mu, e$	$l = \tau$	$l = \mu, e$	$l = \tau$	$l = \mu, e$	$l = \tau$		
[1.1, 6.0]	-0.288(59)	-	-0.132(41)	-	-0.170(119)	-		
[6.0, 8.0]	-0.338(91)	-	-0.450(18)	-	-0.013(13)	-		
[11.0, 12.5]	-0.449(50)	-	-0.401(12)	-	-0.198(73)	-		
[15.0, 17.0]	-0.773(19)	-0.789(18)	-0.270(11)	-0.263(11)	-0.265(46)	-0.257(44)		

q^2 bins (GeV^2)	$\langle P'_4 \rangle$		$\langle P'_5 \rangle$		$10^2 \times \langle P'_6 \rangle$		$10 \times \langle P'_8 \rangle$	
Lepton Mode:	$l = \mu, e$	$l = \tau$	$l = \mu, e$	$l = \tau$	$l = \mu, e$	$l = \tau$	$l = \mu, e$	$l = \tau$
[1.1, 6.0]	0.811(98)	-	-0.520(96)	-	-4.759(390)	-	0.1492(118)	-
[6.0, 8.0]	1.116(41)	-	-0.801(56)	-	-2.011(159)	-	0.0205(18)	-
[11.0, 12.5]	1.180(22)	-	-0.705(34)	-	-1.547(89)	-	-0.1146(74)	-
[15.0, 17.0]	1.317(8)	0.524(8)	-0.432(19)	-0.162(8)	-1.296(92)	-0.505(39)	-0.0436(46)	-0.0156(18)

Table 17: q^2 averaged estimates of clean observables $P_i^{(')}$ in separate q^2 bins.

uncertainties of $P_{1,2,3}$ are larger compared to $P'_{4,5,6,8}$, especially in the low q^2 bins. This is due to the large error estimate that was obtained for $S_{3,6s,9}$ in table 14. The reported uncertainties for these observables are to be viewed as conservative estimates.

The results presented in this work provide a comprehensive analysis of the angular observables associated with the $B_c^- \rightarrow D_s^{*-} (\rightarrow D_s^- \pi^0) \ell^+ \ell^-$ decay within the SM framework, for both light and heavy lepton modes. Recently, LHCb performed a detailed angular analysis of a related decay mode $B \rightarrow K^* \ell^+ \ell^-$, where they reported a deviation of about 3.0σ from SM predictions in P_2 and P'_5 [56] in the third q^2 bin. It is thus motivating to establish precise SM predictions of these observables for B_c decay modes. These predictions will serve as benchmarks once future experimental measurements on the $B_c^- \rightarrow D_s^{*-} \ell^+ \ell^-$ become available. Any significant deviation from the SM predictions could hint towards possible NP contributions.

6 Summary and Conclusions

In this work, we have studied some rare decay modes of the B_c meson in the SM. In the framework of pQCD, we have utilized the available lattice inputs on $B_s \rightarrow D_s^{(*)}$ and $B_c \rightarrow D_s$ form factors and extracted the shape parameters of the B_c and $D_s^{(*)}$ meson wave functions, which in turn define the pQCD form factors. We have obtained the following values of the shape parameters associated with B_c and B_s meson wave functions:

$$\omega_{B_c} = 1.011(60), \quad \omega_{B_s} = 0.491(31). \quad (6.1)$$

Similarly, for the D_s and D_s^* meson wave functions we obtain

$$C_{D_s} = 0.496(66), \quad C_{D_s^*} = 0.505(44), \quad (6.2)$$

and

$$\omega_{D_s} = 0.101(11), \quad \omega_{D_s^*} = 0.099(14). \quad (6.3)$$

We find our estimate of ω_{B_c} to be in good agreement with our previous estimates presented in [19, 20], thereby reinforcing the consistency of our methodology. Using these shape parameters, we can parameterize the wavefunction of the participating mesons. Furthermore, using these wave functions and the HQSS relations between $B_c \rightarrow D_s$ and $B_c \rightarrow D_s^*$ form factors, we have extracted the q^2 shapes of the $B_c \rightarrow D_s^*$ form factors. With this information we have then predicted a number of several observables, like branching fractions, lepton flavor universality ratios, and various angular observables, associated with the $B_c^- \rightarrow D_s^{*-} \ell^+ \ell^-$ and $B_c^- \rightarrow D_s^{*-} \nu \bar{\nu}$ FCNC decays.

A Expressions of various transversity amplitudes in $B_c^- \rightarrow D_s^{*-} \ell^+ \ell^-$

In this section, we present the detailed mathematical expression of the transversity amplitudes on which the angular coefficients defined in eq. 2.8 are dependent.

$$\begin{aligned}
\mathcal{A}_\perp^{L,R} &= -N_\ell \sqrt{2N_{D_s^*}} \sqrt{\lambda(m_{B_c}^2, m_{D_s^*}^2, q^2)} \left[(C_9^{eff} \mp C_{10}) \frac{V(q^2)}{m_{B_c} + m_{D_s^*}} + 2\hat{m}_b C_7^{eff} T_1(q^2) \right], \\
\mathcal{A}_\parallel^{L,R} &= N_\ell \sqrt{2N_{D_s^*}} \left[(C_9^{eff} \mp C_{10})(m_{B_c} + m_{D_s^*}) A_1(q^2) + 2\hat{m}_b C_7^{eff} (m_{B_c}^2 - m_{D_s^*}^2) T_2(q^2) \right], \\
\mathcal{A}_0^{L,R} &= \frac{N_\ell \sqrt{N_{D_s^*}}}{2m_{D_s^*} \sqrt{q^2}} \left[(C_9^{eff} \mp C_{10}) \left\{ (m_{B_c}^2 - m_{D_s^*}^2 - q^2)(m_{B_c} + m_{D_s^*}) A_1(q^2) - \frac{\lambda(m_{B_c}^2, m_{D_s^*}^2, q^2)}{m_{B_c} + m_{D_s^*}} A_2(q^2) \right\} \right. \\
&\quad \left. + 2m_b C_7^{eff} \left\{ (m_{B_c}^2 + 3m_{D_s^*}^2 - q^2) T_2(q^2) - \frac{\lambda(m_{B_c}^2, m_{D_s^*}^2, q^2)}{m_{B_c}^2 - m_{D_s^*}^2} T_3(q^2) \right\} \right], \\
\mathcal{A}_t(q^2) &= 2N_\ell \sqrt{N_{D_s^*}} \sqrt{\frac{\lambda(m_{B_c}^2, m_{D_s^*}^2, q^2)}{q^2}} C_{10} A_0(q^2),
\end{aligned} \tag{A.1}$$

with $\hat{m}_b = m_b/q^2$, $\beta_\ell = \sqrt{1 - 4m_\ell^2/q^2}$, and the normalization factors are expressed as

$$\begin{aligned}
N_\ell &= \frac{i\alpha_e G_F}{4\sqrt{2}\pi} V_{tb} V_{ts}^*, \\
N_{D_s^*} &= \frac{8\sqrt{\lambda}q^2}{3 \times 256\pi^3 m_{B_c}^3} \sqrt{1 - \frac{4m_\ell^2}{q^2}} \mathcal{B}(D_s^{*-} \rightarrow D_s^- \pi^0),
\end{aligned} \tag{A.2}$$

with $\mathcal{B}(D_s^{*-} \rightarrow D_s^- \pi^0) = 5.77(35)\%$ [38]. These transversity amplitudes depend on the WCs and the QCD form factors. The Wilson coefficients $C_{7,9}^{eff}(\mu)$ in Eqn (A.1) have the form [57, 58]

$$\begin{aligned}
C_7^{eff}(\mu) &= C_7(\mu) + i\alpha_s(\mu) \left[\frac{2}{9} \eta^{14/23} \left\{ \frac{x_t(x_t^2 - 5x_t - 2)}{8(x_t - 1)^3} + \frac{3x_t^2 \ln(x_t)}{4(x_t - 1)^4} - 0.1687 \right\} - 0.03C_2(\mu) \right], \\
C_9^{eff}(q^2, \mu) &= C_9(\mu) + Y_{pert}(q^2, \mu) + Y_{res}(q^2, \mu),
\end{aligned} \tag{A.3}$$

with $x_t = m_t^2/m_W^2$ and $\eta = \alpha_s(m_W)/\alpha_s(\mu)$ with $\alpha_s(\mu)$ being calculated at $\mu = m_b$. The short distance contributions from the soft gluon emission, and the one loop contribution from the four Fermi operators O_{1-6} are collected in the $Y_{pert}(q^2, \mu)$ part of $C_9^{eff}(\mu)$ and

C_1	C_2	C_3	C_4	C_5	C_6	C_7	C_8	C_9	C_{10}
-0.175	1.076	0.01258	-0.03279	0.01112	-0.03634	-0.302	-0.148	4.232	-4.410

Table 18: Numerical values of Wilson coefficients C_{1-10} evaluated at m_b scale [24].

can be written as [59]

$$\begin{aligned}
Y_{pert}(\hat{s}, \mu) = & 0.124\omega(\hat{s}) + g(\hat{m}_c, \hat{s})C(\mu) + \lambda_u [g(\hat{m}_c, \hat{s}) - g(0, \hat{s})] (3C_1(\mu) + C_2(\mu)) \\
& - \frac{1}{2}g(0, \hat{s})(C_3(\mu) + 3C_4(\mu)) - \frac{1}{2}g(1, \hat{s})(4C_3(\mu) + 4C_4(\mu) + 3C_5(\mu) + C_6(\mu)) \\
& + \frac{2}{9}(3C_3(\mu) + C_4(\mu) + 3C_5(\mu) + C_6(\mu)),
\end{aligned} \tag{A.4}$$

where $\hat{s} = q^2/m_b^2$, $\hat{m}_c = m_c/m_b$, $\lambda_u = (V_{ub}V_{us}^*)/(V_{tb}V_{ts}^*)$ and $C(\mu) = 3C_1(\mu) + C_2(\mu) + 3C_3(\mu) + C_4(\mu) + 3C_5(\mu) + C_6(\mu)$, with the Wilson Coefficients $C_{1-10}(\mu)$ being evaluated upto the next to leading order correction at $\mu = m_b$ scale. The numerical values of the Wilson coefficients at m_b scale [24, 58] that have been used in this work are tabulated in table 18.

In addition, in eq.(A.4), the term $\omega(\hat{s})$ representing the one gluon correction to the matrix element of the operator O_9 is represented as [23, 58, 59]

$$\begin{aligned}
\omega(\hat{s}) = & -\frac{2}{9}\pi^2 + \frac{4}{3}\int_0^{\hat{s}} \frac{\ln(1-u)}{u} du - \frac{2}{3}\ln(\hat{s})\ln(1-\hat{s}) - \frac{5+4\hat{s}}{3(1+2\hat{s})}\ln(1-\hat{s}) \\
& - \frac{2\hat{s}(1+\hat{s})(1-2\hat{s})}{3(1-\hat{s})^2(1+2\hat{s})}\ln(\hat{s}) + \frac{5+9\hat{s}-6\hat{s}^2}{6(1-\hat{s})(1+2\hat{s})}.
\end{aligned} \tag{A.5}$$

The functions $g(z, \hat{s})$ and $g(0, \hat{s})$ in eqn.(A.4) representing the one loop contributions of the O_{1-6} are represented as [59]

$$g(z, \hat{s}) = -\frac{8}{9}\ln(z) + \frac{8}{27} + \frac{4}{9}x - \frac{2}{9}(2+x)\sqrt{|1-x|} \times \begin{cases} \ln|\frac{1+\sqrt{1-x}}{1-\sqrt{1-x}}| - i\pi & \text{for } x \equiv \frac{4z^2}{\hat{s}} < 1 \\ 2\arctan(\frac{1}{\sqrt{x-1}}) & \text{for } x \equiv \frac{4z^2}{\hat{s}} > 1, \end{cases} \tag{A.6}$$

and

$$g(0, \hat{s}) = \frac{8}{27} - \frac{8}{9}\ln(\frac{m_b}{\mu}) - \frac{4}{9}\ln(\hat{s}) + \frac{4}{9}i\pi, \tag{A.7}$$

and $\lambda_u = V_{ub}V_{us}^*/V_{tb}V_{ts}^*$. In addition to $Y_{pert}(q^2, \mu)$, the third term $Y_{res}(q^2, \mu)$ in eqn.(A.3) describes the long distance contributions to $C_9^{eff}(\mu)$ and is associated with intermediate light vector mesons, i.e., ρ , ω and ϕ mesons, and vector charmonium mesons, i.e., J/ψ and $\psi(2S)$ is expressed as [59, 60]

$$\begin{aligned}
Y_{res}(q^2, \mu) = & -\frac{3\pi}{\alpha_e^2} \left\{ C(\mu) \sum_{V_i=J/\psi, \psi(2S)} \frac{m_{V_i} \mathcal{B}(V_i \rightarrow \ell^+ \ell^-) \Gamma_{V_i}}{q^2 - m_{V_i}^2 + im_{V_i} \Gamma_{V_i}} \right. \\
& \left. - \lambda_u g(0, \hat{s})(3C_1(\mu) + C_2(\mu)) \sum_{V_i=\rho, \phi, \omega} \frac{m_{V_i} \mathcal{B}(V_i \rightarrow \ell^+ \ell^-) \Gamma_{V_i}}{q^2 - m_{V_i}^2 + im_{V_i} \Gamma_{V_i}} \right\},
\end{aligned} \tag{A.8}$$

where m_{V_i} and Γ_{V_i} represent the mass and the total decay width of the vector meson V_i respectively, and $\mathcal{B}(V_i \rightarrow \ell^+ \ell^-)$ is the branching ratio of each of the dilepton decay mode. We have used the numerical values of these parameters as input in this work [38] and present them in table 19. It is to be noted that the last two rows in this equation represent the

Intermediate Meson V_i	m_{V_i} in MeV	Γ_{V_i} in MeV	$\mathcal{B}(V_i \rightarrow \ell^+ \ell^-)$ with	
			$l = \mu$	$l = \tau$
ρ	775.26(23)	147.4(8)	$4.55(28) \times 10^{-5}$	-
ω	782.66(13)	8.68(13)	$7.4(1.8) \times 10^{-5}$	-
ϕ	1019.461(16)	4.249(13)	$2.85(19) \times 10^{-4}$	-
J/ψ	3096.900(6)	0.0926(17)	$5.961(33) \times 10^{-2}$	-
$\psi(2S)$	3686.10(6)	0.294(8)	$8.0(6) \times 10^{-3}$	$3.1(4) \times 10^{-3}$
$\psi(3770)$	3773.7(7)	27.2(1.0)	$9.6(7) \times 10^{-6}$	-
$\psi(4040)$	4040.0(4.0)	84.0(12.0)	$1.02(17) \times 10^{-5}$	-

Table 19: Masses, total decay widths and dilepton branching fractions of the intermediate vectors mesons.

dilepton branching fractions of $\psi(3770)$ and $\psi(4040)$ inspite of lying in the physical q^2 range, offer negligible contribution to Y_{res} , and their effects are smeared out in q^2 distribution of the observables, something that we will showcase in the results section. This is primarily because their dilepton decay widths are highly suppressed compared to that of J/ψ and $\psi(2S)$.

B Expressions of form factors in PQCD approach

In this appendix, we present the analytical expressions of the form factors already discussed in 2.2.

- For $B_s \rightarrow D_s$ transition the auxiliary form factors $f_1(q^2)$ and $f_2(q^2)$ have the analytic forms [34]

$$f_1(q^2) = 8\pi m_{B_s}^2 C_F \int_0^1 dx_1 dx_2 \int_0^{b_c} b_1 db_1 b_2 db_2 \phi_{B_s}(x_1, b_1) \phi_{D_s}(x_2, b_2) \left\{ [2r(1 - rx_2)] \cdot H_1(t_1) + \left[2r(2r_c - r) + x_1 r \left(-2 + 2\eta + \sqrt{\eta^2 - 1} - \frac{2\eta}{\sqrt{\eta^2 - 1}} + \frac{\eta^2}{\sqrt{\eta^2 - 1}} \right) \right] \cdot H_2(t_2) \right\}, \quad (\text{B.1})$$

$$f_2(q^2) = 8\pi m_{B_s}^2 C_F \int_0^1 dx_1 dx_2 \int_0^{b_c} b_1 db_1 b_2 db_2 \phi_{B_s}(x_1, b_1) \phi_{D_s}(x_2, b_2)$$

$$\left\{ [2 - 4x_2r(1 - \eta)] \cdot H_1(t_1) + \left[4r - 2r_c - x_1 + \frac{x_1}{\sqrt{\eta^2 - 1}}(2 - \eta) \right] \cdot H_2(t_2) \right\}.$$

- For $B_s \rightarrow D_s^*$ transition the axial-vector and vector form factors $A_{0,1,2}(q^2)$ and $V(q^2)$ respectively have the analytic forms [34]

$$\begin{aligned} A_0(q^2) &= 8\pi m_{B_s}^2 C_F \int_0^1 dx_1 dx_2 \int_0^{b_c} b_1 db_1 b_2 db_2 \phi_{B_s}(x_1, b_1) \phi_{D_s^*}(x_2, b_2) \\ &\quad \left\{ [1 + r - rx_2(2 + r - 2\eta)] \cdot H_1(t_1) \right. \\ &\quad \left. + \left[r^2 + r_c + \frac{x_1}{2} + \frac{\eta x_1}{2\sqrt{\eta^2 - 1}} + \frac{rx_1}{2\sqrt{\eta^2 - 1}}(1 - 2\eta(\eta + \sqrt{\eta^2 - 1})) \right] \cdot H_2(t_2) \right\}, \\ A_1(q^2) &= 8\pi m_{B_s}^2 C_F \int_0^1 dx_1 dx_2 \int_0^{b_c} b_1 db_1 b_2 db_2 \phi_{B_s}(x_1, b_1) \phi_{D_s^*}(x_2, b_2) \frac{r}{1+r} \\ &\quad \left\{ 2[1 + \eta - 2rx_2 + r\eta x_2] \cdot H_1(t_1) + [2r_c + 2\eta r - x_1] \cdot H_2(t_2) \right\}, \quad (\text{B.2}) \\ A_2(q^2) &= \frac{(1+r)^2(\eta-r)}{2r(\eta^2-1)} A_1(q^2) \\ &\quad - 8\pi m_{B_s}^2 C_F \int_0^1 dx_1 dx_2 \int_0^{b_c} b_1 db_1 b_2 db_2 \phi_{B_s}(x_1, b_1) \phi_{D_s^*}(x_2, b_2) \frac{1+r}{\eta^2-1} \\ &\quad \times \left\{ [(1+\eta)(1-r) - rx_2(1-2r+\eta(2+r-2\eta))] \cdot H_1(t_1) \right. \\ &\quad \left. + \left[r + r_c(\eta-r) - \eta r^2 + rx_1\eta^2 - \frac{x_1}{2}(\eta+r) + x_1(\eta r - \frac{1}{2})\sqrt{\eta^2-1} \right] \cdot H_2(t_2) \right\}, \\ V(q^2) &= 8\pi m_{B_s}^2 C_F \int_0^1 dx_1 dx_2 \int_0^{b_c} b_1 db_1 b_2 db_2 \phi_{B_s}(x_1, b_1) \phi_{D_s^*}(x_2, b_2) (1+r) \\ &\quad \left\{ [1 - rx_2] \cdot H_1(t_1) + \left[r + \frac{x_1}{2\sqrt{\eta^2-1}} \right] \cdot H_2(t_2) \right\}. \end{aligned}$$

- For $B_c \rightarrow D_s$ transition the auxiliary form factors $f_1(q^2)$ and $f_2(q^2)$ and the tensor form factor $F_T(q^2)$ have the following analytic forms [26]

$$\begin{aligned} f_1(q^2) &= 16\pi m_{B_c}^2 r C_F \int_0^1 dx_1 dx_2 \int_0^{b_c} b_1 db_1 b_2 db_2 \phi_{B_c}(x_1, b_1) \phi_{D_s}(x_2, b_2) \\ &\quad \times \left\{ [1 - rx_2] \cdot H_1(t_1) - [r + 2x_1(1 - \eta)] \cdot H_2(t_2) \right\}, \end{aligned}$$

$$f_2(q^2) = 16\pi m_{B_c}^2 C_F \int_0^1 dx_1 dx_2 \int_0^{b_c} b_1 db_1 b_2 db_2 \phi_{B_c}(x_1, b_1) \phi_{D_s}(x_2, b_2)$$

$$\times \left\{ [1 - 2rx_2(1 - \eta)] \cdot H_1(t_1) + [2r - x_1] \cdot H_2(t_2) \right\}, \quad (\text{B.3})$$

$$F_T(q^2) = 8\pi m_{B_c}^2 (1+r) C_F \int_0^1 dx_1 dx_2 \int_0^{b_c} b_1 db_1 b_2 db_2 \phi_{B_c}(x_1, b_1) \phi_{D_s}(x_2, b_2) \\ \times \left\{ [1 - rx_2] \cdot H_1(t_1) + [2r - x_1] \cdot H_2(t_2) \right\}.$$

- For $B_c \rightarrow D_s^*$ transition the axial-vector and vector form factors $A_{0,1,2}(q^2)$ and $V(q^2)$ respectively have the analytic forms [26]

$$A_0(q^2) = 8\pi m_{B_c}^2 C_F \int_0^1 dx_1 dx_2 \int_0^{b_c} b_1 db_1 b_2 db_2 \phi_{B_c}(x_1, b_1) \phi_{D_s^*}(x_2, b_2) \\ \left\{ [1 - rx_2(r - 2\eta) + r(1 - 2x_2)] \cdot H_1(t_1) + [r^2 + x_1(1 - 2r\eta)] \cdot H_2(t_2) \right\},$$

$$A_1(q^2) = 16\pi m_{B_c}^2 C_F \frac{r}{1+r} \int_0^1 dx_1 dx_2 \int_0^{b_c} b_1 db_1 b_2 db_2 \phi_{B_c}(x_1, b_1) \phi_{D_s^*}(x_2, b_2) \\ \left\{ [1 + rx_2\eta - 2rx_2 + \eta] \cdot H_1(t_1) + [r\eta - x_1] \cdot H_2(t_2) \right\},$$

$$A_2(q^2) = \frac{(1+r)^2(\eta-r)}{2r(\eta^2-1)} A_1(q^2) \quad (\text{B.4}) \\ - 8\pi m_{B_c}^2 C_F \frac{1+r}{\eta^2-1} \int_0^1 dx_1 dx_2 \int_0^{b_c} b_1 db_1 b_2 db_2 \phi_{B_c}(x_1, b_1) \phi_{D_s^*}(x_2, b_2) \\ \times \left\{ [\eta(1 - r^2 x_2) - rx_2(1 - 2\eta^2 - 2r) + (1 - r) - r\eta(1 + 2x_2)] \cdot H_1(t_1) \right. \\ \left. + [r(1 - x_1 + 2x_1\eta^2) - \eta(r^2 + x_1)] \cdot H_2(t_2) \right\},$$

$$V(q^2) = 8\pi m_{B_c}^2 C_F \int_0^1 dx_1 dx_2 (1+r) \int_0^{b_c} b_1 db_1 b_2 db_2 \phi_{B_c}(x_1, b_1) \phi_{D_s^*}(x_2, b_2) \\ \left\{ [1 - rx_2] \cdot H_1(t_1) + r \cdot H_2(t_2) \right\},$$

and the tensor form factors $T_{1,2,3}$ have the analytic forms [26]

$$T_1(q^2) = 8\pi m_{B_c}^2 C_F \int_0^1 dx_1 dx_2 \int_0^{b_c} b_1 db_1 b_2 db_2 \phi_{B_c}(x_1, b_1) \phi_{D_s^*}(x_2, b_2) \\ \left\{ [1 + r(1 - x_2(2 + r - 2\eta))] \cdot H_1(t_1) + [r(1 - x_1)] \cdot H_2(t_2) \right\},$$

$$T_2(q^2) = 16\pi m_{B_c}^2 C_F \frac{r}{1-r^2} \int_0^1 dx_1 dx_2 (1+r) \int_0^{b_c} b_1 db_1 b_2 db_2 \phi_{B_c}(x_1, b_1) \phi_{D_s^*}(x_2, b_2)$$

$$\begin{aligned} & \left\{ [(1-r)(1+\eta) + 2rx_2(r-\eta) + rx_2(2\eta^2 - r\eta - 1)] \cdot H_1(t_1) \right. \\ & \left. + [r(1+x_1)\eta - r^2 - x_1] \cdot H_2(t_2) \right\}, \end{aligned} \quad (\text{B.5})$$

$$\begin{aligned} T_3(q^2) = & \frac{r+\eta}{r} \frac{1-r^2}{2(\eta^2-1)} T_2(q^2) - \frac{1-r^2}{\eta^2-1} \\ & \times 8\pi m_{B_c}^2 C_F \int_0^1 dx_1 dx_2 \int_0^{b_c} b_1 db_1 b_2 db_2 \phi_{B_c}(x_1, b_1) \phi_{D_s^*}(x_{2,b_2}) \\ & \times \left\{ [1 + rx_2(\eta - 2) + \eta] \cdot H_1(t_1) + [x_1\eta - r] \cdot H_2(t_2) \right\}. \end{aligned}$$

In all the above expressions $r = m/M$, $r_{b(c)} = m_{b(c)}/M$, and

$$H_i(t_i) = \alpha_s(t_i) h_i(x_1, x_2, b_1, b_2) \exp[-S_{ab}(t_i)], \quad (\text{B.6})$$

with $\alpha_s(t)$, $h_i(x_1, x_2, b_1, b_2)$ and $S_{ab}(t)$ representing the strong coupling constant evaluated at scale t , the hard kernel and the Sudakov factor respectively. The detailed expressions for these terms are presented in the following appendix.

C Scales and relevant functions in the hard kernel

In this appendix, we present analytic expressions for the hard functions and scales. The hard kernel h_i comes from the Fourier transform of virtual quark and gluon propagators

$$\begin{aligned} h_1(x_1, x_2, b_1, b_2) = & K_0(\beta_1 b_1) \left[\theta(b_1 - b_2) I_0(\alpha_1 b_2) K_0(\alpha_1 b_1) \right. \\ & \left. + \theta(b_2 - b_1) I_0(\alpha_1 b_1) K_0(\alpha_1 b_2) \right] S_t(x_2), \\ h_2(x_1, x_2, b_1, b_2) = & K_0(\beta_2 b_2) \left[\theta(b_1 - b_2) I_0(\alpha_2 b_2) K_0(\alpha_2 b_1) \right. \\ & \left. + \theta(b_2 - b_1) I_0(\alpha_2 b_1) K_0(\alpha_2 b_2) \right] S_t(x_1), \end{aligned} \quad (\text{C.1})$$

where K_0 and I_0 are the modified Bessel functions, and

$$\begin{aligned} \alpha_1 = & m_{B_s} \sqrt{x_2 r \eta^+}, \\ \alpha_2 = & m_{B_s} \sqrt{x_1 r \eta^+ - r^2 + r_c^2}, \\ \beta_{1,2} = & m_{B_s} \sqrt{x_1 x_2 r \eta^+}, \end{aligned} \quad (\text{C.2})$$

for form factors of $B_s \rightarrow D_s^{(*)}$ form factors in eqns.(B.1)-(B.2) and taken from [34, 61], and

$$\begin{aligned}\alpha_1 &= m_{B_c} \sqrt{2rx_2\eta + r_b^2 - 1 - r^2x_2^2}, \\ \alpha_2 &= m_{B_c} \sqrt{rx_1\eta^+ + r_c^2 - r^2}, \\ \beta_{1,2} &= m_{B_c} \sqrt{x_1x_2r\eta^+ - r^2x_2^2},\end{aligned}\tag{C.3}$$

for form factors of $B_c \rightarrow D_s^{(*)}$ decays shown in eqns.(B.3)-(B.5) and taken from [62]. In addition to the hard kernels in Eqn (B.6) the Sudakov factors $S_{ab}(t)$ evaluated in modified PQCD framework has been taken from [32]. The hard scale t is chosen to be the maximum of the virtuality of internal momentum transition in the hard amplitudes

$$\begin{aligned}t_1 &= \max(\alpha_1, 1/b_1, 1/b_2), \\ t_2 &= \max(\alpha_2, 1/b_1, 1/b_2),\end{aligned}\tag{C.4}$$

and the jet function $S_t(x)$ has the same form as Eqn (2.29).

D Inputs utilized in this work

In this appendix we present the inputs of $B_s \rightarrow D_s^{(*)}$ and $B_c \rightarrow D_s$ form factors at discrete w values, or more fundamentally q^2 values, which has been used in the chi-square minimizations we performed in this work.

- In table 20, we present lattice inputs for $B_c \rightarrow D_s$ form factors at $w = 1.0, 1.15$ and 1.3 . These have been used to extract the soft function coefficients in table 7.

Form Factors at w	Value from HPQCD	Correlation								
		$F_+(1.0)$	$F_+(1.15)$	$F_+(1.3)$	$F_0(1.0)$	$F_0(1.15)$	$F_0(1.3)$	$F_T(1.0)$	$F_T(1.15)$	$F_T(1.3)$
$F_+(1.0)$	1.464(128)	1.0	0.945	0.664	-0.062	0.234	0.228	0.061	0.053	0.021
$F_+(1.15)$	0.830(50)		1.0	0.862	-0.077	0.295	0.340	0.067	0.068	0.035
$F_+(1.3)$	0.527(23)			1.0	-0.075	0.322	0.525	0.063	0.084	0.066
$F_0(1.0)$	0.737(11)				1.0	0.659	0.338	0.095	0.093	0.043
$F_0(1.15)$	0.512(8)					1.0	0.799	0.061	0.090	0.063
$F_0(1.3)$	0.385(8)						1.0	0.038	0.092	0.102
$F_T(1.0)$	2.032(64)							1.0	0.511	0.103
$F_T(1.15)$	1.208(31)								1.0	0.829
$F_T(1.3)$	0.787(31)									1.0

Table 20: HPQCD inputs for $B_c \rightarrow D_s$ form factors, along-with their correlation

- In tables 21 and 22, we present inputs for rest of the $B_c \rightarrow D_s^*$ form factors generated using the soft function parameters extracted in table 7. We have treated each form factor as uncorrelated with the others. This was done because all the form factors were derived from the same universal functions Σ_1 and Σ_2 , which made the full correlation matrix positive semidefinite and led to numerical instability during chi-square minimization in table 11. So to avoid this we have considered all the form factors to be uncorrelated.

Form Factors	Value Obtained	Correlation			Form Factors	Value Obtained	Correlation		
		$A_0(1.0)$	$A_0(1.15)$	$A_0(1.3)$			$A_1(1.0)$	$A_1(1.15)$	$A_1(1.3)$
$A_0(1.0)$	2.554(39)	1.0	0.659	0.296	$A_1(1.0)$	0.746(11)	1.0	0.700	0.397
$A_0(1.15)$	1.367(19)		1.0	0.728	$A_1(1.15)$	0.496(9)		1.0	0.816
$A_0(1.3)$	0.816(18)			1.0	$A_1(1.3)$	0.363(10)			1.0
Form Factors	Value Obtained	Correlation			Form Factors	Value Obtained	Correlation		
		$A_{12}(1.0)$	$A_{12}(1.15)$	$A_{12}(1.3)$			$V(1.0)$	$V(1.15)$	$V(1.3)$
$A_{12}(1.0)$	0.246(4)	1.0	0.702	0.443	$V(1.0)$	2.165(136)	1.0	0.704	0.207
$A_{12}(1.15)$	0.176(4)		1.0	0.828	$V(1.15)$	1.243(60)		1.0	0.823
$A_{12}(1.3)$	0.140(5)			1.0	$V(1.3)$	0.788(35)			1.0

Table 21: Inputs for $B_c \rightarrow D_s^*$ axial-vector and vector form factors $A_{0,1,2}$ and V obtained using soft function parameters extracted in this work.

Form Factors	Value Obtained	Correlation			Form Factors	Value Obtained	Correlation		
		$T_1(1.0)$	$T_1(1.15)$	$T_1(1.3)$			$T_2(1.0)$	$T_2(1.15)$	$T_2(1.3)$
$T_1(1.0)$	1.571(31)	1.0	0.669	0.204	$T_2(1.0)$	0.745(11)	1.0	0.702	0.367
$T_1(1.15)$	0.901(14)		1.0	0.805	$T_2(1.15)$	0.534(8)		1.0	0.780
$T_1(1.3)$	0.574(12)			1.0	$T_2(1.3)$	0.411(8)			1.0
Form Factors	Value Obtained	Correlation							
		$T_{23}(1.0)$	$T_{23}(1.15)$	$T_{23}(1.3)$					
$T_{23}(1.0)$	0.991(14)	1.0	0.639	0.360					
$T_{23}(1.15)$	0.557(15)		1.0	0.823					
$T_{23}(1.3)$	0.355(20)			1.0					

Table 22: Synthetic data for $B_c \rightarrow D_s^*$ tensor form factors $T_{1,2,3}$ obtained using soft function parameters extracted in this work.

E Correlation matrices

In this appendix, we present the correlation matrices obtained between the extracted parameters in each of the chi-square optimizations.

- In table 23, we present the correlation matrix between the LCDA shape parameters of B_s , B_c and $D_s^{(*)}$ mesons, whose values we had extracted and showcased in table 5.

	ω_{B_c}	ω_{B_s}	C_{D_s}	$C_{D_s^*}$	ω_{D_s}	$\omega_{D_s^*}$	m_b	m_c	$\delta_{f_1}^{B_s \rightarrow D_s}$	$\delta_{f_2}^{B_s \rightarrow D_s}$	$\delta_{A_0}^{B_s \rightarrow D_s^*}$	$\delta_{A_1}^{B_s \rightarrow D_s^*}$	$\delta_V^{B_s \rightarrow D_s}$	$\delta_{f_1}^{B_c \rightarrow D_s}$	$\delta_{f_2}^{B_c \rightarrow D_s}$	$\delta_{F_T}^{B_c \rightarrow D_s}$
ω_{B_c}	1.0	0.659	0.792	0.622	0.072	-0.047	0.027	-0.018	0.090	0.002	-0.046	0.166	-0.445	0.411	0.076	0.172
ω_{B_s}		1.0	0.574	0.487	-0.015	-0.009	0.055	-0.012	0.088	-0.018	-0.002	0.125	-0.334	0.291	0.026	0.145
C_{D_s}			1.0	0.648	-0.105	-0.043	0.039	-0.114	0.078	0.015	-0.074	0.199	-0.467	0.384	-0.016	0.213
$C_{D_s^*}$				1.0	-0.285	-0.007	0.009	-0.240	0.066	0.018	-0.081	0.188	-0.398	0.267	-0.145	0.228
ω_{D_s}					1.0	-0.002	-0.294	0.279	0.057	-0.064	0.138	-0.147	0.047	0.128	0.386	-0.152
$\omega_{D_s^*}$						1.0	-0.040	0.040	0.937	-0.666	0.409	-0.496	-0.435	-0.060	-0.221	0.512
m_b							1.0	0.812	0.057	-0.042	0.055	-0.088	0.098	0.095	0.294	-0.151
m_c								1.0	0.169	-0.072	0.294	-0.314	0.115	0.193	0.412	-0.237
$\delta_{f_1}^{B_s \rightarrow D_s}$									1.0	-0.738	0.463	-0.513	-0.609	-0.001	-0.160	0.484
$\delta_{f_2}^{B_s \rightarrow D_s}$										1.0	0.051	-0.087	0.687	0.548	-0.378	-0.718
$\delta_{A_0}^{B_s \rightarrow D_s^*}$											1.0	-0.569	-0.000	0.611	-0.538	-0.199
$\delta_{A_1}^{B_s \rightarrow D_s^*}$												1.0	-0.032	-0.376	0.498	0.238
$\delta_V^{B_s \rightarrow D_s}$													1.0	0.272	-0.163	-0.774
$\delta_{f_1}^{B_c \rightarrow D_s}$														1.0	-0.539	-0.588
$\delta_{f_2}^{B_c \rightarrow D_s}$															1.0	0.318
$\delta_{F_T}^{B_c \rightarrow D_s}$																1.0

Table 23: Correlation Matrix between the extracted LCDA parameters and nuisance parameters.

- In table 24, we present the correlation matrix between the seven $B_c \rightarrow D_s^*$ semileptonic form factors at $q^2 = 0$ predicted in table 6.

	$A_0(0)$	$A_1(0)$	$A_2(0)$	$V(0)$	$T_1(0)$	$T_2(0)$	$T_3(0)$
$A_0(0)$	1.0	0.052	0.067	0.036	0.038	0.040	0.042
$A_1(0)$		1.0	0.083	0.040	0.049	0.052	0.054
$A_2(0)$			1.0	0.051	0.057	0.061	0.063
$V(0)$				1.0	0.028	0.031	0.030
$T_1(0)$					1.0	0.036	0.039
$T_2(0)$						1.0	0.040
$T_3(0)$							1.0

Table 24: Correlation matrix between the $B_c \rightarrow D_s^*$ form factors calculated at $q^2 = 0$.

- In table 25, we present the correlation matrix between the BGL coefficients of $B_c \rightarrow D_s^*$ form factors extracted in table 11.

	$a_0^{A_0}$	$a_1^{A_0}$	$a_2^{A_0}$	$a_0^{A_1}$	$a_1^{A_1}$	$a_2^{A_1}$	$a_1^{A_{12}}$	$a_2^{A_{12}}$	a_0^V	a_1^V	a_2^V	$a_0^{T_1}$	$a_1^{T_1}$	$a_2^{T_1}$	$a_1^{T_2}$	$a_2^{T_2}$	$a_0^{T_{23}}$	$a_1^{T_{23}}$	$a_2^{T_{23}}$
$a_0^{A_0}$	1.0	0.3362	-0.1359	0.0012	0.0019	0.0016	0.4590	0.3455	0.0013	0.0015	0.0002	0.0003	0.0005	0.0003	0.0006	0.0005	0.0004	0.0006	0.0005
$a_1^{A_0}$		1.0	0.5511	0.0023	0.0036	0.0030	0.8767	0.6600	0.0025	0.0028	0.0005	0.0006	0.0010	0.0006	0.0011	0.0009	0.0008	0.0011	0.0009
$a_2^{A_0}$			1.0	0.0018	0.0029	0.0024	0.6940	0.5225	0.0020	0.0022	0.0004	0.0005	0.0008	0.0004	0.0009	0.0007	0.0006	0.0008	0.0007
$a_0^{A_1}$				1.0	0.4805	0.0766	0.0024	0.0018	0.0018	0.0020	0.0003	0.0005	0.0008	0.0005	0.0010	0.0007	0.0007	0.0009	0.0008
$a_1^{A_1}$					1.0	0.7629	0.0038	0.0029	0.0028	0.0031	0.0005	0.0008	0.0013	0.0007	0.0015	0.0011	0.0014	0.0012	
$a_2^{A_1}$						1.0	0.0032	0.0024	0.0024	0.0026	0.0004	0.0007	0.0011	0.0006	0.0013	0.0010	0.0009	0.0012	0.0010
$a_1^{A_{12}}$							1.0	0.7019	0.0026	0.0030	0.0005	0.0006	0.0010	0.0006	0.0012	0.0009	0.0009	0.0011	0.0010
$a_2^{A_{12}}$								1.0	0.0020	0.0022	0.0004	0.0005	0.0008	0.0004	0.0009	0.0007	0.0006	0.0008	0.0007
a_0^V									1.0	0.5234	-0.1874	0.0005	0.0007	0.0004	0.0008	0.0006	0.0007	0.0009	0.0008
a_1^V										1.0	-0.0167	0.0005	0.0008	0.0005	0.0009	0.0007	0.0008	0.0010	0.0009
a_2^V											1.0	0.0001	0.0001	0.0001	0.0002	0.0001	0.0001	0.0002	0.0001
$a_0^{T_1}$												1.0	0.1705	-0.3199	0.4178	0.3145	0.0002	0.0002	0.0002
$a_1^{T_1}$													1.0	0.0477	0.6807	0.5125	0.0003	0.0004	0.0003
$a_2^{T_1}$														1.0	0.3796	0.2858	0.0002	0.0002	0.0002
$a_1^{T_2}$															1.0	0.5392	0.0003	0.0004	0.0004
$a_2^{T_2}$																1.0	0.0002	0.0003	0.0003
$a_0^{T_{23}}$																	1.0	0.6942	0.3281
$a_1^{T_{23}}$																		1.0	0.8415
$a_2^{T_{23}}$																			1.0

Table 25: Correlation between extracted BGL parameters of $B_c \rightarrow D_s^*$ form factors (with A_{12} and T_{23}).

References

- [1] CDF collaboration, *Observation of the B_c meson in $p\bar{p}$ collisions at $\sqrt{s} = 1.8$ TeV*, *Phys. Rev. Lett.* **81** (1998) 2432 [[hep-ex/9805034](#)].
- [2] M. Pepe Altarelli and F. Teubert, *B Physics at LHCb*, *Int. J. Mod. Phys. A* **23** (2008) 5117 [[0802.1901](#)].
- [3] CDF collaboration, *Search for the flavor-changing neutral current decays $B^+ \rightarrow \mu^+ \mu^- K^+$ and $B^0 \rightarrow \mu^+ \mu^- K^{*0}$* , *Phys. Rev. Lett.* **83** (1999) 3378 [[hep-ex/9905004](#)].
- [4] BELLE collaboration, *Observation of the decay $B \rightarrow K\ell^+\ell^-$* , *Phys. Rev. Lett.* **88** (2002) 021801 [[hep-ex/0109026](#)].
- [5] BELLE collaboration, *Observation of $B \rightarrow K^* l^+ l^-$* , *Phys. Rev. Lett.* **91** (2003) 261601 [[hep-ex/0308044](#)].
- [6] BELLE collaboration, *Measurement of the Differential Branching Fraction and Forward-Backward Asymmetry for $B \rightarrow K^{(*)}\ell^+\ell^-$* , *Phys. Rev. Lett.* **103** (2009) 171801 [[0904.0770](#)].
- [7] BELLE collaboration, *Lepton-Flavor-Dependent Angular Analysis of $B \rightarrow K^*\ell^+\ell^-$* , *Phys. Rev. Lett.* **118** (2017) 111801 [[1612.05014](#)].
- [8] BELLE collaboration, *Test of lepton flavor universality and search for lepton flavor violation in $B \rightarrow K\ell\ell$ decays*, *JHEP* **03** (2021) 105 [[1908.01848](#)].
- [9] BELLE collaboration, *Test of Lepton-Flavor Universality in $B \rightarrow K^*\ell^+\ell^-$ Decays at Belle*, *Phys. Rev. Lett.* **126** (2021) 161801 [[1904.02440](#)].
- [10] BABAR collaboration, *Evidence for the rare decay $B \rightarrow K^*\ell^+\ell^-$ and measurement of the $B \rightarrow K\ell^+\ell^-$ branching fraction*, *Phys. Rev. Lett.* **91** (2003) 221802 [[hep-ex/0308042](#)].
- [11] BABAR collaboration, *Direct CP, Lepton Flavor and Isospin Asymmetries in the Decays $B \rightarrow K^{(*)}\ell^+\ell^-$* , *Phys. Rev. Lett.* **102** (2009) 091803 [[0807.4119](#)].
- [12] BABAR collaboration, *Measurement of Branching Fractions and Rate Asymmetries in the Rare Decays $B \rightarrow K^{(*)}\ell^+\ell^-$* , *Phys. Rev. D* **86** (2012) 032012 [[1204.3933](#)].
- [13] CMS collaboration, *Angular analysis of the decay $B^0 \rightarrow K^{*0}\mu^+\mu^-$ from pp collisions at $\sqrt{s} = 8$ TeV*, *Phys. Lett. B* **753** (2016) 424 [[1507.08126](#)].
- [14] LHCb collaboration, *Differential branching fraction and angular analysis of the $B^+ \rightarrow K^+\mu^+\mu^-$ decay*, *JHEP* **02** (2013) 105 [[1209.4284](#)].
- [15] LHCb collaboration, *Measurement of Form-Factor-Independent Observables in the Decay $B^0 \rightarrow K^{*0}\mu^+\mu^-$* , *Phys. Rev. Lett.* **111** (2013) 191801 [[1308.1707](#)].
- [16] LHCb collaboration, *Test of lepton universality using $B^+ \rightarrow K^+\ell^+\ell^-$ decays*, *Phys. Rev. Lett.* **113** (2014) 151601 [[1406.6482](#)].
- [17] LHCb collaboration, *Test of lepton universality with $B^0 \rightarrow K^{*0}\ell^+\ell^-$ decays*, *JHEP* **08** (2017) 055 [[1705.05802](#)].
- [18] LHCb collaboration, *Test of lepton universality in beauty-quark decays*, *Nature Phys.* **18** (2022) 277 [[2103.11769](#)].
- [19] U. Dey and S. Nandi, *Correlated study on some $B_c \rightarrow P$ and $B_c \rightarrow S$ wave channels in light of new inputs*, *JHEP* **07** (2025) 144 [[2503.01693](#)].

[20] U. Dey and S. Nandi, *Study of Form Factors and Observables in $B_c^- \rightarrow \bar{D}^{(*)0} \ell^- \bar{\nu}_\ell$ and $B_c^- \rightarrow D^{(*)-} \ell^+ \ell^-$ decays*, [2509.19445](#).

[21] W. Altmannshofer, P. Ball, A. Bharucha, A.J. Buras, D.M. Straub and M. Wick, *Symmetries and Asymmetries of $B \rightarrow K^* \mu^+ \mu^-$ Decays in the Standard Model and Beyond*, *JHEP* **01** (2009) 019 [[0811.1214](#)].

[22] A. Ali, P. Ball, L.T. Handoko and G. Hiller, *A Comparative study of the decays $B \rightarrow (K, K^*) \ell^+ \ell^-$ in standard model and supersymmetric theories*, *Phys. Rev. D* **61** (2000) 074024 [[hep-ph/9910221](#)].

[23] W.-F. Wang and Z.-J. Xiao, *The semileptonic decays $B/B_s \rightarrow (\pi, K)(\ell^+ \ell^-, \ell \nu, \nu \bar{\nu})$ in the perturbative QCD approach beyond the leading-order*, *Phys. Rev. D* **86** (2012) 114025 [[1207.0265](#)].

[24] G. Buchalla, A.J. Buras and M.E. Lautenbacher, *Weak decays beyond leading logarithms*, *Rev. Mod. Phys.* **68** (1996) 1125 [[hep-ph/9512380](#)].

[25] T. Barakat, *Fourth generation effects on the rare $B \rightarrow K^*$ neutrino anti-neutrino decay*, *New J. Phys.* **4** (2002) 25 [[hep-ph/0105116](#)].

[26] W.-F. Wang, X. Yu, C.-D. Lü and Z.-J. Xiao, *Semileptonic decays $B_c^+ \rightarrow D_{(s)}^{(*)}(l^+ \nu_l, l^+ l^-, \nu \bar{\nu})$ in the perturbative qcd approach*, *Phys. Rev. D* **90** (2014) 094018.

[27] J. Matias, F. Mescia, M. Ramon and J. Virto, *Complete Anatomy of $\bar{B}_d \rightarrow \bar{K}^{*0}(- \rightarrow K\pi) l^+ l^-$ and its angular distribution*, *JHEP* **04** (2012) 104 [[1202.4266](#)].

[28] S. Descotes-Genon, T. Hurth, J. Matias and J. Virto, *Optimizing the basis of $B \rightarrow K^* ll$ observables in the full kinematic range*, *JHEP* **05** (2013) 137 [[1303.5794](#)].

[29] H.-n. Li and H.-L. Yu, *Perturbative QCD analysis of B meson decays*, *Phys. Rev. D* **53** (1996) 2480 [[hep-ph/9411308](#)].

[30] T. Kurimoto, H.-n. Li and A.I. Sanda, *$B \rightarrow D^{(*)}$ form-factors in perturbative QCD*, *Phys. Rev. D* **67** (2003) 054028 [[hep-ph/0210289](#)].

[31] H.-n. Li, *Threshold resummation for exclusive B meson decays*, *Phys. Rev. D* **66** (2002) 094010 [[hep-ph/0102013](#)].

[32] X. Liu, H.-n. Li and Z.-J. Xiao, *Improved perturbative qcd formalism for B_c meson decays*, *Phys. Rev. D* **97** (2018) 113001.

[33] Z.-J. Xiao, W.-F. Wang and Y.-y. Fan, *Revisiting the pure annihilation decays $B_s \rightarrow \pi^+ \pi^-$ and $B^0 \rightarrow K^+ K^-$: the data and the pQCD predictions*, *Phys. Rev. D* **85** (2012) 094003 [[1111.6264](#)].

[34] X.-Q. Hu, S.-P. Jin and Z.-J. Xiao, *Semileptonic decays $B/B_s \rightarrow (D^{(*)}, D_s^{(*)}) l \nu_l$ in the PQCD approach with the lattice QCD input*, *Chin. Phys. C* **44** (2020) 053102 [[1912.03981](#)].

[35] R.-H. Li, C.-D. Lu and H. Zou, *The $B(B(s)) \rightarrow D(s) P$, $D(s) V$, $D^*(s) P$ and $D^*(s) V$ decays in the perturbative QCD approach*, *Phys. Rev. D* **78** (2008) 014018 [[0803.1073](#)].

[36] C. McNeile, C.T.H. Davies, E. Follana, K. Hornbostel and G.P. Lepage, *Heavy meson masses and decay constants from relativistic heavy quarks in full lattice QCD*, *Phys. Rev. D* **86** (2012) 074503 [[1207.0994](#)].

[37] ETM collaboration, *Masses and decay constants of $D_{(s)}^*$ and $B_{(s)}^*$ mesons with $N_f = 2 + 1 + 1$ twisted mass fermions*, *Phys. Rev. D* **96** (2017) 034524 [[1707.04529](#)].

[38] PARTICLE DATA GROUP collaboration, *Review of particle physics*, *Phys. Rev. D* **110** (2024) 030001.

[39] HPQCD collaboration, *Form factors for the processes $B_c^+ \rightarrow D^0 \ell^+ \nu_\ell$ and $B_c^+ \rightarrow D_s^+ \ell^+ \ell^+ (\nu \bar{\nu})$ from lattice QCD*, *Phys. Rev. D* **105** (2022) 014503 [[2108.11242](#)].

[40] C. Bourrely, I. Caprini and L. Lellouch, *Model-independent description of $B \rightarrow pi l nu$ decays and a determination of $|V(ub)|$* , *Phys. Rev. D* **79** (2009) 013008 [[0807.2722](#)].

[41] E. McLean, C.T.H. Davies, J. Koponen and A.T. Lytle, *$B_s \rightarrow D_s \ell \nu$ Form Factors for the full q^2 range from Lattice QCD with non-perturbatively normalized currents*, *Phys. Rev. D* **101** (2020) 074513 [[1906.00701](#)].

[42] HPQCD collaboration, *$Bs \rightarrow Ds^*$ form factors for the full q^2 range from lattice QCD*, *Phys. Rev. D* **105** (2022) 094506 [[2105.11433](#)].

[43] M. Bordone, N. Gubernari, D. van Dyk and M. Jung, *Heavy-Quark expansion for $\bar{B}_s \rightarrow D_s^{(*)}$ form factors and unitarity bounds beyond the $SU(3)_F$ limit*, *Eur. Phys. J. C* **80** (2020) 347 [[1912.09335](#)].

[44] Y.Y. Keum, H.-N. Li and A.I. Sanda, *Penguin enhancement and $B \rightarrow K\pi$ decays in perturbative QCD*, *Phys. Rev. D* **63** (2001) 054008 [[hep-ph/0004173](#)].

[45] X. Liu, H.-n. Li and Z.-J. Xiao, *Next-to-leading-logarithm k_T resummation for $B_c \rightarrow J/\psi$ decays*, *Phys. Lett. B* **811** (2020) 135892 [[2006.12786](#)].

[46] S. Cheng, Y.-Y. Fan, X. Yu, C.-D. Lü and Z.-J. Xiao, *The NLO twist-3 contributions to $B \rightarrow \pi$ form factors in k_T factorization*, *Phys. Rev. D* **89** (2014) 094004 [[1402.5501](#)].

[47] N. Mahajan, *$B \rightarrow rho$ form-factors including higher twist contributions and reliability of pQCD approach*, [hep-ph/0405161](#).

[48] W. Wang, Y.-L. Shen and C.-D. Lu, *Covariant Light-Front Approach for $B(c)$ transition form factors*, *Phys. Rev. D* **79** (2009) 054012 [[0811.3748](#)].

[49] E.E. Jenkins, M.E. Luke, A.V. Manohar and M.J. Savage, *Semileptonic $B(c)$ decay and heavy quark spin symmetry*, *Nucl. Phys. B* **390** (1993) 463 [[hep-ph/9204238](#)].

[50] P. Colangelo, F. De Fazio and F. Loparco, *Role of $B_c^+ \rightarrow B_{s,d}^{(*)} \bar{\ell} \nu_\ell$ in the Standard Model and in the search for BSM signals*, *Phys. Rev. D* **103** (2021) 075019 [[2102.05365](#)].

[51] A. Biswas, S. Nandi, S.K. Patra and I. Ray, *Study of the $b \rightarrow d \ell \ell$ transitions in the Standard Model and test of New Physics sensitivities*, *JHEP* **03** (2023) 247 [[2208.14463](#)].

[52] A. Bharucha, T. Feldmann and M. Wick, *Theoretical and Phenomenological Constraints on Form Factors for Radiative and Semi-Leptonic B -Meson Decays*, *JHEP* **09** (2010) 090 [[1004.3249](#)].

[53] N. Gubernari, M. Reboud, D. van Dyk and J. Virto, *Dispersive analysis of $B \rightarrow K^{(*)}$ and $B_s \rightarrow \phi$ form factors*, *JHEP* **12** (2023) 153 [[2305.06301](#)].

[54] A. Bharucha, D.M. Straub and R. Zwicky, *$B \rightarrow V \ell^+ \ell^-$ in the Standard Model from light-cone sum rules*, *JHEP* **08** (2016) 098 [[1503.05534](#)].

[55] FLAVOUR LATTICE AVERAGING GROUP (FLAG) collaboration, *FLAG Review 2024*, [2411.04268](#).

[56] LHCb collaboration, *Angular Analysis of the $B^+ \rightarrow K^{*+} \mu^+ \mu^-$ Decay*, *Phys. Rev. Lett.* **126** (2021) 161802 [[2012.13241](#)].

- [57] C.-H. Chen and C.Q. Geng, *Baryonic rare decays of Lambda(b) —> Lambda lepton+ lepton-*, *Phys. Rev. D* **64** (2001) 074001 [[hep-ph/0106193](#)].
- [58] N.R. Soni, A. Issadykov, A.N. Gadaria, J.J. Patel and J.N. Pandya, *Rare b → d decays in covariant confined quark model*, *Eur. Phys. J. A* **58** (2022) 39 [[2008.07202](#)].
- [59] S.-P. Jin, X.-Q. Hu and Z.-J. Xiao, *Study of $B_s \rightarrow K^{(*)}\ell^+\ell^-$ decays in the PQCD factorization approach with lattice QCD input*, *Phys. Rev. D* **102** (2020) 013001 [[2003.12226](#)].
- [60] P. Nayek, P. Maji and S. Sahoo, *Study of semileptonic decays $B \rightarrow \pi l^+l^-$ and $B \rightarrow \rho l^+l^-$ in nonuniversal Z' model*, *Phys. Rev. D* **99** (2019) 013005 [[1811.09991](#)].
- [61] W.-F. Wang, Y.-Y. Fan and Z.-J. Xiao, *Semileptonic decays $B_c \rightarrow (\eta_c, J/\Psi)l\nu$ in the perturbative QCD approach*, *Chin. Phys. C* **37** (2013) 093102 [[1212.5903](#)].
- [62] X.-Q. Hu, S.-P. Jin and Z.-J. Xiao, *Semileptonic decays $B_c \rightarrow (\eta_c, J/\psi)l\bar{\nu}_l$ in the "PQCD + Lattice" approach*, *Chin. Phys. C* **44** (2020) 023104 [[1904.07530](#)].